J Biomol NMR (2012) 54:53–67
DOI 10.1007/s10858-012-9651-4

ARTICLE

Very large residual dipolar couplings from deuterated ubiquitin

Joshua M. Ward · Nikolai R. Skrynnikov

Received: 6 May 2012 / Accepted: 25 June 2012 / Published online: 25 July 2012

Abstract Main-chain $^{1}H^{N}$–^{15}N residual dipolar couplings (RDCs) ranging from approximately −200 to 200 Hz have been measured for ubiquitin under strong alignment conditions in Pf1 phage. This represents a ten-fold increase in the degree of alignment over the typical weakly aligned samples. The measurements are made possible by extensive proton-dilution of the sample, achieved by deuteration of the protein with partial back-substitution of labile protons from 25 % H_2O / 75 % D_2O buffer. The spectral quality is further improved by application of deuterium decoupling. Since standard experiments using fixed-delay INEPT elements cannot accommodate a broad range of couplings, the measurements were conducted using *J*-resolved and *J*-modulated versions of the HSQC and TROSY sequences. Due to unusually large variations in dipolar couplings, the trosy (sharp) and anti-trosy (broad) signals are often found to be interchanged in the TROSY spectra. To distinguish between the two, we have relied on their respective ^{15}N linewidths. This strategy ultimately allowed us to determine the signs of RDCs. The fitting of the measured RDC values to the crystallographic coordinates of ubiquitin yields the quality factor $Q = 0.16$, which confirms the perturbation-free character of the Pf1 alignment. Our results demonstrate that RDC data can be successfully acquired not only in dilute liquid crystals, but also in more concentrated ones. As a general rule, the increase in liquid crystal concentration improves the stability of alignment media and makes them more tolerant to variations in sample conditions. The technical ability to measure RDCs under moderately strong alignment conditions may open the door for development of alternative alignment media, including new types of media that mimic biologically relevant systems.

Keywords Residual dipolar couplings · Alignment media · Deuteration · *J*-resolved and *J*-modulated spectroscopy · HSQC · TROSY · Differential line broadening · Ubiquitin · Pf1 phage

Introduction

Since the day when protein residual dipolar couplings (RDCs) were first observed in solution, the RDC measurements have been conducted in weakly aligned samples (Tolman et al. 1995; Tjandra and Bax 1997). This restriction is one of necessity, because with increasing degree of alignment spectral linewidths become dominated by residual proton–proton couplings. Essentially, by raising the degree of alignment one moves toward the limit of static solid, where proton detection (as customary in solution experiments) suffers from strongly broadened signals. As a consequence, the studies have been limited to weak orienting media and alignment tags, of which a great variety have been developed over the last decade (Prestegard and Kishore 2001; Tolman and Ruan 2006; Su and Otting 2010).

Several strategies have been devised to counter the effect of proton–proton couplings and potentially expand

Electronic supplementary material The online version of this article (doi:10.1007/s10858-012-9651-4) contains supplementary material, which is available to authorized users.

J. M. Ward · N. R. Skrynnikov (✉)
Department of Chemistry, Purdue University, 560 Oval Drive, West Lafayette, IN 47907-2084, USA
e-mail: nikolai@purdue.edu

Present Address:
J. M. Ward
Chemistry Department, University of Oulu, POB 3000, 90014 Oulu, Finland

the scope of RDC experiments. In particular, application of selective proton pulses and homonuclear decoupling have been shown to attenuate the unwanted ^{1}H–^{1}H couplings, allowing for accurate measurements of $^{1}H^{N}$–^{15}N RDCs up to ca. 40 Hz (Vander Kooi et al. 1999; Jensen et al. 2004; de Alba and Tjandra 2006; Furrer et al. 2007; Yao et al. 2009). Borrowing a page from solid-state NMR book, it has been demonstrated that RDCs can be scaled by application of the variable-angle sample spinning (Tian et al. 1999; Zandomeneghi and Meier 2004; Lancelot et al. 2005). Trempe and co-workers recently presented the experiment where the recoupling REDOR sequence is applied to the oriented ubiquitin samples under MAS conditions (Trempe et al. 2008). In this fashion the moderately large (ca. 25 Hz) $^{1}H^{N}$–^{15}N couplings were successfully recovered, whereas ^{1}H–^{1}H couplings were suppressed. One potential complication in such experiments is that the orientation of the liquid–crystalline director can be unstable when the sample is spun at the magic angle (Kishore and Prestegard 2003; Zandomeneghi et al. 2003); this issue can be addressed by preparing polymer-based or polymer-stabilized samples (Trempe et al. 2008).

Another, more conventional strategy that helps to eliminate ^{1}H–^{1}H couplings involves protein deuteration. Deuteration as an avenue to narrow proton lines has a long history in NMR. Typically, this approach involves compromises. For instance, in solution partial deuteration of large proteins leads to sharpening of the NOESY peaks but, at the same time, undercuts their intensity (Torchia et al. 1988; Gardner and Kay 1998). Conventional structure determination methods were shown to perform best at the level of ^{2}H incorporation close to 50 % (Nietlispach et al. 1996). In solids the requirements are more stringent. Spectra with very high resolution can be obtained using perdeuterated samples with 10 % protons back-exchanged into labile sites (Chevelkov et al. 2006). The compromise between resolution and sensitivity in ^{1}H–^{15}N correlation experiments is reached at 30–40 % proton content in the labile sites (Akbey et al. 2010).

In our RDC study we take a cue from these recently developed solid-state approaches. It has been widely recognized that protein deuteration improves both precision and accuracy of RDC measurements in weak alignment media (Wang et al. 1998; de Alba and Tjandra 2006; Yao et al. 2008). Here we seek to demonstrate that high degree of deuteration also allows for measurement of unusually large RDCs under strong alignment conditions (order parameter ca. 10^{-2}). Our specific aim was to reliably measure $^{1}H^{N}$–^{15}N couplings in the range of several hundred Hz—one order of magnitude higher than is normally measured with standard weakly aligning media.

The increased magnitude of RDCs in our experiments does not necessarily translate into better precision. Indeed, the improvement is offset by relatively low sensitivity (due to partial substitution of $^{2}H^{N}$ for $^{1}H^{N}$) and the remaining amount of line-broadening. As it turns out, the precision of our experiments is in line with (high-quality) data obtained from the traditional weakly oriented media. Instead, our study seeks to create additional opportunities for development of protein alignment media.

While many existing protein media have an excellent success record, no single media can suit all situations. For instance, DHPC/DMPC bicelles have a restrictive temperature range (Ottiger and Bax 1998), Pf1 phage tends to associate with positively charged proteins (Hansen et al. 1998), and PEG/hexanol does not allow for accurate prediction of protein alignment (Yuwen et al. 2011). On the other hand, there exists a large class of alignment media for small organic molecules that give rise to very large RDCs (Emsley and Lindon 1975). Recently, several new media have been developed that produce a moderately strong and scalable degree of alignment in organic molecules (Luy et al. 2004; Thiele 2005). This leads us to believe that eventually such media can also be discovered for proteins. Here we seek to demonstrate that such hypothetical media will be viable from the perspective of NMR measurements. Indeed, as shown in our report, $^{1}H^{N}$–^{15}N RDCs on the order of 200 Hz can be reliably measured in the deuterated protein samples.

In this connection it should be pointed out that moderately strong alignment should be especially useful for obtaining long-range distance restraints. In isotropic solution, it has been demonstrated that methyl–methyl distances of up to 12 Å can be measured in the deuterated samples with selective proton incorporation (Sounier et al. 2007). In the weakly oriented media, $^{1}H^{N}$–$^{1}H^{N}$ RDCs measured in deuterated samples translate into distances >7 Å (Wu and Bax 2002; Meier et al. 2003; Schanda et al. 2007) or, alternatively, allow for detection of transient $^{1}H^{N}$–$^{1}H^{N}$ contacts in disordered protein (Meier et al. 2007). It can be envisaged that the use of new methyl labeling schemes (Lichtenecker et al. 2004; Goto et al. 1999) in concert with strong protein alignment, as explored in this report, will allow for measurement of extremely long proton–proton distances.

Finally, there is another area where the methods developed in this work can prove to be useful. In certain experimental applications the alignment media is itself a target of biological interest and therefore cannot be replaced or easily modified. For example, Koenig et al. developed a system based on rhodopsin-rich retinal disk membranes which spontaneously align in an external magnetic field. This system has been used to study transient binding of a fragment from G protein transducin to rhodopsin receptor (Koenig et al. 2002). In a similar vein, Chen et al. (2005) investigated association of inhibitor peptides with Aβ fibrils. The RDCs

measured in this context have been termed "transferred dipolar couplings". In a hypothetical scenario where such couplings turn out to be too large and cannot be scaled down by dilution (see below), one may also take advantage of the methods developed in this study.

Materials and methods

Protein sample preparation

^{15}N-labeled ubiquitin samples were expressed and purified according to the standard protocol adapted from (Lazar et al. 1997). Perdeuterated ^{2}H,^{15}N-labeled ubiquitin was expressed on Spectra9 minimal media (CIL, > 98 % ^{2}H, > 97 % ^{15}N). Prior to expression, BL21(DE3) cells were conditioned for growth in D_2O (Li et al. 2002). The protein material was dissolved in 75 % D_2O / 25 % H_2O, 10 mM sodium phosphate, 50 mM NaCl, pH 7.0 buffer. Back-exchange of amide protons was achieved by 4 h incubation at 75 °C followed by an overnight refolding at room temperature. Residual protonation at non-exchangeable sites was estimated to be 2–3 %, based on the integrated signal intensities (amide vs. methyl regions in the 1D spectra of the protonated and deuterated samples). The Pf1 phage (ASLA Biotech) was first exchanged into NMR buffer (Hansen et al. 1998) (two rounds of buffer exchange, centrifuged at 50,000 rpm/150,000*g*, 3 h, 4 °C). Measured volume of stock Pf1 solution was then added to the protein sample to obtain the following sample conditions: 20 mg/ml Pf1 phage, 50 mM NaCl, 1.7 mM ubiquitin [corresponding to 0.4 mM content of $^{1}H^{N}$ (LiWang and Bax 1996)].

NMR spectroscopy

All spectra were recorded at 25 °C on an 800 MHz Bruker Avance III spectrometer equipped with room temperature triple-resonance probe and z-axis gradients. Reference $^{1}J_{NH}$ couplings were obtained from ^{1}H,^{15}N IPAP-HSQC spectra (Ottiger et al. 1998) of ^{2}H,^{15}N ubiquitin in 90 % H_2O. Note that measurements of RDCs in the strongly aligned sample cannot be readily conducted using the standard techniques. Indeed, in this situation the net couplings $\Sigma = {}^{1}J_{NH} + {}^{1}D_{NH}$ vary widely from residue to residue and strongly deviate from the nominal $^{1}J_{NH}$ value of ca. −90 Hz. This means that one single setting of the INEPT delay τ cannot reasonably accommodate the entire array of Σ values. As a consequence, many resonances in the standard HSQC spectra become weak or disappear altogether while other resonances are inverted. Furthermore, the in-phase/anti-phase separation scheme in the IPAP sequence is disrupted for majority of residues.

To address this problem we have implemented a *J*-resolved version of ^{1}H,^{15}N HSQC, where the INEPT delay τ is incremented in concert with the ^{15}N chemical shift evolution delay t_1 (see Fig. S1). The concept of this experiment is reminiscent of the *J*-resolved HMBC (Furihata and Seto 1999). The signal derived from this sequence is proportional to

$$I(t_1) \sim \sin^2\left(\pi\Sigma\frac{t_1}{2}\right)\exp(i\omega_{0N}t_1) \sim$$
$$\sim -\frac{1}{2}\left\{\exp\left(i\left(\omega_{0N}+2\pi\frac{\Sigma}{2}\right)t_1\right) - 2\exp(i\omega_{0N}t_1)\right.$$
$$\left. + \exp\left(i\left(\omega_{0N}-2\pi\frac{\Sigma}{2}\right)t_1\right)\right\} \quad (1)$$

which corresponds to a triplet pattern in the ^{15}N dimension, with (1):(−2):(1) intensity ratio and splitting between the outer components equal to $|\Sigma|$.

In addition, we have implemented a *J*-modulated ^{1}H,^{15}N HSQC experiment (Fig. S2), which is similar to the ones previously reported (Tjandra et al. 1996; Tolman and Prestegard 1996). In brief, a series of seven 2D correlation maps are recorded, each with a different INEPT delay time $\tau = 1/(4\Sigma_0)$ (Σ_0 = 45, 60, 90, 120, 180, 360, and 720 Hz). In the case of conventional HSQC sequence, shortening of the INEPT delays preclude the use of water flip-back pulses and refocusing gradients, which leads to unsatisfactory water suppression. In contrast, the sensitivity-enhanced sequence with gradient encoding (Kay et al. 1992) retains good water suppression properties even for very short τ. Consequently, we chose this sequence as a basis for our *J*-modulated experiment (Fig. S2). The modulation of peak intensity (volume) in this experiment can be expressed as (Cavanagh et al. 2007):

$$I(\tau) = I_0\sin^2(\pi\Sigma 2\tau)\exp\left(-2R_{2,eff}2\tau\right)\left\{\frac{1+\exp\left(-R_{2,eff}2\tau\right)}{2}\right\} \quad (2)$$

Here $R_{2,eff}$ is the effective transverse relaxation rate during the INEPT delays (see caption of Tab. S1 for more accurate description of $R_{2,eff}$), and the factor in curly brackets reflects the presence of two distinct magnetization transfer pathways in the sensitivity enhancement scheme (Cavanagh et al. 2007).

Similarly, we have implemented the *J*-modulated versions of the ^{1}H,^{15}N TROSY HSQC sequence (Fig. S3). As a starting point, we used the sensitivity-enhanced version of TROSY with gradient selection (Nietlispach 2005). Not surprisingly, the coherence selection scheme works well for those residues for which Σ matches the current setting

Table 1 Relative intensities (volumes) of the four components of $^{1}H^{N}$–^{15}N quartet in the TROSY experiment Fig. S3 as a function of the variable INEPT duration 2τ

	$H_- + 2H_-N_z$ (broad)	$H_- - 2H_-N_z$ (sharp)
$N_- + 2N_-H_z$ (broad)	$(1/4)\sin(\pi\Sigma 2\tau)(\sin(\pi\Sigma 2\tau)+1)^2$	$-(1/4)\sin(\pi\Sigma 2\tau)\cos^2(\pi\Sigma 2\tau)$
$N_- - 2N_-H_z$ (sharp)	$(1/4)\sin(\pi\Sigma 2\tau)\cos^2(\pi\Sigma 2\tau)$	$-(1/4)\sin(\pi\Sigma 2\tau)(\sin(\pi\Sigma 2\tau)-1)^2$

The entries in this 2 × 2 table are arranged such as to match the positions of the peaks in the *conventional* TROSY spectrum (e.g. the entry in the lower right corner corresponds to the sharp trosy peak, the entry in the upper left corner corresponds to the broad anti-trosy peak, etc.). For those sites where the sign of the net coupling is reversed, $\Sigma = {}^{1}J_{NH} + {}^{1}D_{NH} > 0$, the components of the quartet are interchanged (e.g. trosy peak appears in the upper left corner, anti-trosy peak in the lower right corner, etc.). Note that the sharp component of the proton doublet is $H_- - 2H_-N_z$ (contrary to what is indicated in a number of publications). In order to correctly predict the outcome of this experiment and derive the above results, one has to keep in mind that nitrogen *y*-pulse has a sense of rotation which is opposite to that of the proton *y*-pulse, whereas the respective *x* pulses have the same sense of rotation (Levitt 1997). The complete expressions, containing transverse relaxation rate $R_{2,eff}$, are given in Tab. S1

of τ, $1/(4|\Sigma|) \approx \tau$. For other residues the coherence selection is disrupted, resulting in observation of quartet patterns in the TROSY spectra. The relative intensities of the four quartet components are listed in Table 1. In practice, we found that despite the presence of extra peaks, the TROSY data are usable and useful (see below). In particular, the frequency shifts between the HSQC and TROSY peaks allowed for precise and accurate determination of Σ (Kontaxis et al. 2000). In the following discussion we distinguish between the "TROSY peak" (any peak that appears in the spectra recorded via the pulse sequence Fig. S3) and "trosy peak" (the sharpest component in the $^{1}H^{N}$–^{15}N quartet). Along the same lines, "anti-trosy peak" refers to the broadest component in the $^{1}H^{N}$–^{15}N quartet.

In addition, we have also coded the *J*-modulated IPAP sequence (Ottiger et al. 1998). Similar to TROSY, the coherence selection scheme breaks down for those residues (spectra) that do not meet the $1/(4|\Sigma|) \approx \tau$ condition. This leads to appearance of unwanted doublets in the IPAP spectra. The IPAP data were collected after the TROSY data and thus found redundant; we do not discuss this experiment in the remainder of the paper.

In all experiments we have found that ^{2}H decoupling during the acquisition time greatly improves the quality of spectra [GARP sequence (Shaka et al. 1985), 1.1 kHz *rf* field strength]. We attribute this effect to the presence of sizeable $^{1}H^{N}$–^{2}H RDCs, which can reach ca. 20 Hz in the strongly aligned samples investigated in our study. Note that similar deuterium decoupling strategies have been in use in liquid-crystal NMR of small molecules (Hewitt et al. 1973) and in solids (Pines et al. 1976). On the other hand, the attempted ^{2}H decoupling during the INEPT periods did not seem to be helpful. Indeed, the presence of the refocusing 180° pulse in the middle of the INEPT element largely eliminates the evolution under $^{1}H^{N}$–^{2}H residual dipolar couplings.

As expected, the ^{1}H magnetization recovery is very slow in our heavily deuterated sample. The optimal recycling delay was found to be 4 s, allowing for reasonably short acquisition times (approximately 1 h for HSQC plane and 2 h for TROSY plane). In principle, it should be possible to reduce the measurement time by use of paramagnetic relaxation agents (Eletsky et al. 2003; Cai et al. 2006).

Data analysis

For the strongly aligned ubiquitin sample standard 3D assignment experiments are impracticable due to the INEPT inefficiencies. Instead, the spectra were assigned based on published assignments for ubiquitin in bicelles (Cornilescu et al. 1998), 15 mg/ml Pf1 400 mM NaCl, and 17 mg/ml Pf1 350 mM NaCl (Lakomek et al. 2006). The assignment transfer was aided by the spectra collected from two additional ubiquitin samples, 12 mg/ml Pf1 150 mM NaCl and 20 mg/ml Pf1 460 mM NaCl. In this manner, 44 out of 73 potentially observable residues have been identified. The assignment could in principle be extended on the basis of observed dipolar couplings and their fit to the existing structures (Hus et al. 2002). However, we prefer to avoid any possible circular reasoning and thus limit ourselves to the subset of the readily assignable peaks.

All spectra were processed using NMRPipe (Delaglio et al. 1995). A shifted sine-bell window function was applied in both dimensions, followed by zero-filling. We have found that this standard processing scheme does not interfere with determination of peak widths, which is necessary to distinguish between trosy and anti-trosy peaks (see below). Peak widths, intensities, and frequencies have been determined using the *autofit* routine from the NMRPipe package. In doing so, 2D spectra are processed individually and then stacked to form a pseudo-3D spectrum. Each signal is then fitted using 11 adjustable parameters: two peak center coordinates, two linewidths, and seven peak heights corresponding to the individual planes. The fitted peak volumes $I(\tau_n)$ are obtained from the *autofit* output (VOL or, equivalently, $XW * YW * HEIGHT * Z_n$). The peak positions and intensities determined with the help of *autofit* have been used to determine the magnitude of Σ.

In particular, $I(\tau_n)$ data have been fitted with Eq. (2) using a two-step protocol. First, we conducted a grid search with respect to $|\Sigma|$ combined with simplex minimization in the space of $I_0, R_{2,eff}$. The results were subsequently used as the initial guess for three-parameter $|\Sigma|, I_0, R_{2,eff}$ minimization.

The experimentally determined RDCs were fitted to crystallographic structure 1UBQ (Vijay-Kumar et al. 1987). The structure has been protonated using *hbuild* facility of XPLOR-NIH 2.21 (Schwieters et al. 2003) under CHARMM22 force field (Brooks et al. 2009) and subsequently subjected to 200 rounds of Powell minimization to optimize proton positions (heavy atoms were fixed). During this treatment all interaction parameters were kept at their default values, except *e14fac* which was set to 0.4 (Brunger 1992). The resulting coordinates were used to fit the RDC data with the help of the program PALES (Zweckstetter 2008) The quality of the fit is appreciably better than in the case of the structure protonated by means of the program MOLMOL (Koradi et al. 1996) based on standard protein geometry (quality factor 0.160 vs. 0.206). There is no evidence, however, that this improvement is statistically significant. One should keep in mind that existing *in silico* procedures for protonation of crystal structures can bring about a considerable amount of error (Ulmer et al. 2003).

Results and discussion

As a model system to demonstrate the feasibility of measuring very large $^1H^N$–^{15}N RDCs, we have chosen ubiquitin in solution with Pf1 phage. RDCs on the order of 100 Hz have been previously noted, but not quantified, in this system using the deuterated protein and low ionic strength buffer (Zweckstetter and Bax 2001). At sufficiently high concentration, Pf1 phage generally tends to induce strong alignment in neutral or basic proteins (Ojennus et al. 1999). Unless screened out by salt, electrostatic attraction between the protein and the negatively charged phage particles leads to transient binding which, in turn, produces a high degree of alignment.

For the strongly aligned ubiquitin sample, deuteration provides a dramatic gain in observable signal relative to a standard protonated sample. To illustrate this point we show a side-by-side comparison of the two HSQC spectra from ^1H,^{15}N ubiquitin sample in 12 mg/ml Pf1, 25 mM NaCl, 90 % H_2O / 10 % D_2O[1] and comparable ^2H,^{15}N ubiquitin sample in 20 mg/ml Pf1, 50 mM NaCl, 25 % H_2O / 75 % D_2O. While the first spectrum features a single peak (from the flexible C-terminal residue G76), the second spectrum displays ca. 30 discernible resonances, Fig. S4.

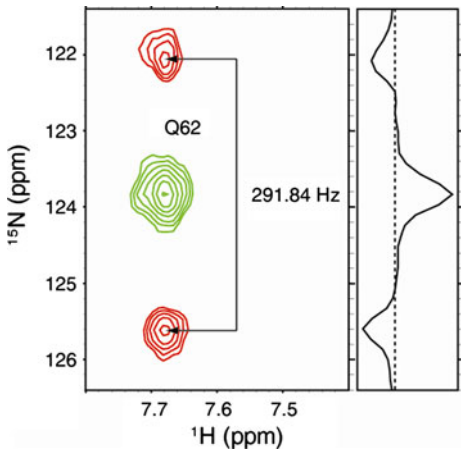

Fig. 1 The triplet pattern of residue Q62 from the *J*-resolved ^1H,^{15}N HSQC spectrum (full spectrum is shown in Fig. S5). The separation between the outer components is equal to $|\Sigma| = |^1J_{NH} + {}^1D_{NH}|$. The spectrum has been recorded in 5 h with 128 complex points in t_1 domain

While deuteration largely eliminates the deleterious effect of proton–proton RDCs, it does not help to resolve the problem of inefficient INEPT transfer in a system with a large spread of $\Sigma = {}^1J_{NH} + {}^1D_{NH}$ couplings. Residues where Σ values strongly deviate from the nominal value of 90 Hz produce weak or unobservable correlations in the regular HSQC spectrum. To address this issue, we have implemented the well-known *J*-resolved and *J*-modulated measurement schemes.

J-resolved ^1H,^{15}N HSQC

The example of large ^1H–^{15}N coupling, as directly observed in the *J*-resolved HSQC spectrum, is shown in Fig. 1. The figure shows a triplet pattern from residue Q62 with the intensity ratio (1):(−2):(1). The net coupling is measured from the separation between the outer components of the triplet, $|\Sigma| = |^1J_{NH} + {}^1D_{NH}| = 291.8$ Hz. Given that the isotropic $^1J_{NH}$ constant is −92.9 Hz, this result allows for two possibilities: $\Sigma = -291.8$ Hz, $^1D_{NH} = -198.9$ Hz or, alternatively, $\Sigma = 291.8$ Hz, $^1D_{NH} = 384.7$ Hz. Unfortunately, the data at hand cannot distinguish between these two scenarios. In any event, the observed coupling is an order of magnitude larger than RDCs typically measured in proteins. In what follows we show how the sign of Σ can be determined, thus yielding the unique value of $^1D_{NH}$ (in the case of Q62, the value of −198.9 Hz proves to be relevant).

The *J*-resolved HSQC is a good scouting experiment as it captures the entire range of RDCs in a single 2D map (full spectrum is shown in Fig. S5). Nevertheless, the spectral map

[1] In this case strong alignment is achieved due to low ionic strength of the solvent.

is obviously crowded and suffers from cancelation effects involving the triplet components of the opposite sign. The unwanted central component arises from the necessity to use two INEPT-derived transfer periods, $\sin^2(\pi\Sigma t_1/2) = (1/2) - (1/2)\cos(\pi\Sigma t_1)$.[2] This feature is reminiscent of the unwanted zero-frequency signal in the recoupled dipolar spectra in solids (Chevelkov et al. 2009; Veglia and Gopinath 2010). In particular, when the coupling Σ is comparable to or smaller than ^{15}N linewidth, the central component of the triplet partially cancels the outer components, which complicates the quantitative determination of Σ.

Some of the problems faced by 2D *J*-resolved HSQC can be alleviated by recording a 3D spectrum, where the INEPT delay τ is used as an extra temporal domain which encodes Σ evolution. The modulation $\Sigma(\tau)$ can be either Fourier-transformed or, alternatively, analyzed in the time domain (Tjandra et al. 1996; Hohwy et al. 2000; Luy and Marino 2003). The latter approach corresponds to the *J*-modulated scheme, as discussed later in the text.

Deuterium decoupling

Given the magnitude of the observed $^1H^N$–^{15}N RDCs (Fig. 1), it is easy to estimate that $^1H^N$–^2H interactions in this strongly aligned deuterated sample can also produce sizable RDCs, up to ~20 Hz. Since there are many such couplings, their net effect is the broadening of $^1H^N$ signals. The broadening can be eliminated by application of deuterium decoupling during the acquisition period. As illustrated in Fig. 2, ^{2}H decoupling indeed leads to significant sharpening of proton resonances, producing approximately twofold gain in signal-to-noise ratio (the peak heights increase, on average, by a factor 1.9 ± 0.6). The decoupling of deuterium-proton dipolar interactions has been widely practiced in strong alignment media (Hewitt et al. 1973; Schenker et al. 1987; Levante et al. 1996), in solid-state MAS experiments (Agarwal and Reif 2008), and even in static solids (Pines et al. 1976). Note that ^{2}H decoupling during the INEPT periods produces no further improvement in spectral quality since ^{1}H–^{2}H dipolar interactions are sufficiently well removed by 180° proton pulse in the middle of the INEPT element.

J-modulated experiments

A *J*-modulated ^{1}H,^{15}N HSQC experiment involves a series of 2D spectra, each recorded with a different INEPT delay τ. Overlaying all spectra collected in this fashion recovers a nearly complete set of ubiquitin resonances (Fig. 3a). 58 out of 73 potentially observable amide peaks can be identified with sufficient degree of confidence. The reasons for the absence of 15 spectral correlations are discussed later in the text.

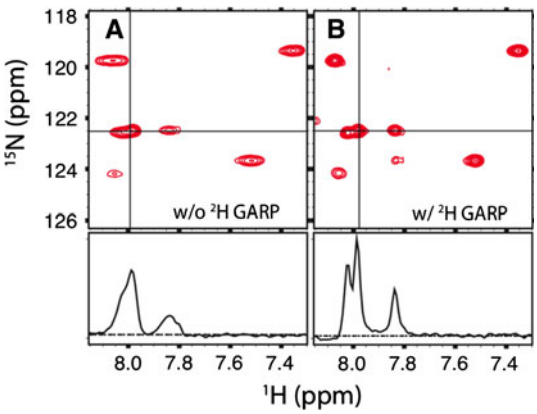

Fig. 2 Selected region in HSQC spectra of ^{2}H,^{15}N ubiquitin strongly aligned in Pf1 phage; the spectra have been recorded (**a**) without and (**b**) with the application of 1.1 kHz GARP ^{2}H decoupling during the acquisition time. In the latter case, ^{2}H decoupling has been applied concurrently with the standard ^{15}N decoupling (1.3 kHz GARP, length of the acquisition period 80 ms)

Signal intensities in the *J*-modulated HSQC experiment display the expected oscillatory pattern, $\sin^2(\pi\Sigma 2\tau)$, as illustrated for residue Q62 (Figs. 3b–h). The extracted peak volumes fit well to the theoretical dependence, Eq. 2. In the case of Q62, curve fitting yields $|\Sigma| = 281.4$ Hz (Fig. 3i), which is in decent agreement with the value 291.8 Hz determined from the *J*-resolved HSQC (Fig. 1). Similar high-quality fits have been obtained for other HSQC peaks (Fig. S6).

A *J*-modulated TROSY series was recorded in the same fashion, i.e. by incrementing the INEPT delays τ in the regular pulse sequence. The TROSY coherence selection scheme performs well when the setting of τ approximately matches $1/(4|\Sigma|)$ for a given residue. However, for those 2D planes where τ significantly deviates from $1/(4|\Sigma|)$, the selection scheme fails and other quartet components emerge in the spectra. This is illustrated in Fig. 4 panels (b–h) which contain the signals from residue Q62. In particular, two substantial peaks appear in these plots (at the opposite corners of the dashed-line contour), which can be identified as trosy and anti-trosy components.

Of note, in our experiment it may not be trivial to distinguish between trosy and anti-trosy peaks. Indeed, if the net coupling Σ is negative, i.e. has the same sign as $^1J_{NH} \approx -90$ Hz, then the trosy peak appears below and to the right of the HSQC resonance (similar to conventional spectra). However, if Σ is positive then trosy peak is found in an unusual quadrant—above and to the left of the HSQC

[2] Because of the wide scatter in the values of Σ and the rapid loss of magnetization during the transfer, we cannot separate the *transfer* stage from the *modulation* stage, as has been done in other sequences (Tjandra et al. 1996; Kelly et al. 1996). For the same reasons we did not use the correction strategies such as *J*-mismatch compensation (Schanda et al. 2007; Nielsen et al. 1989).

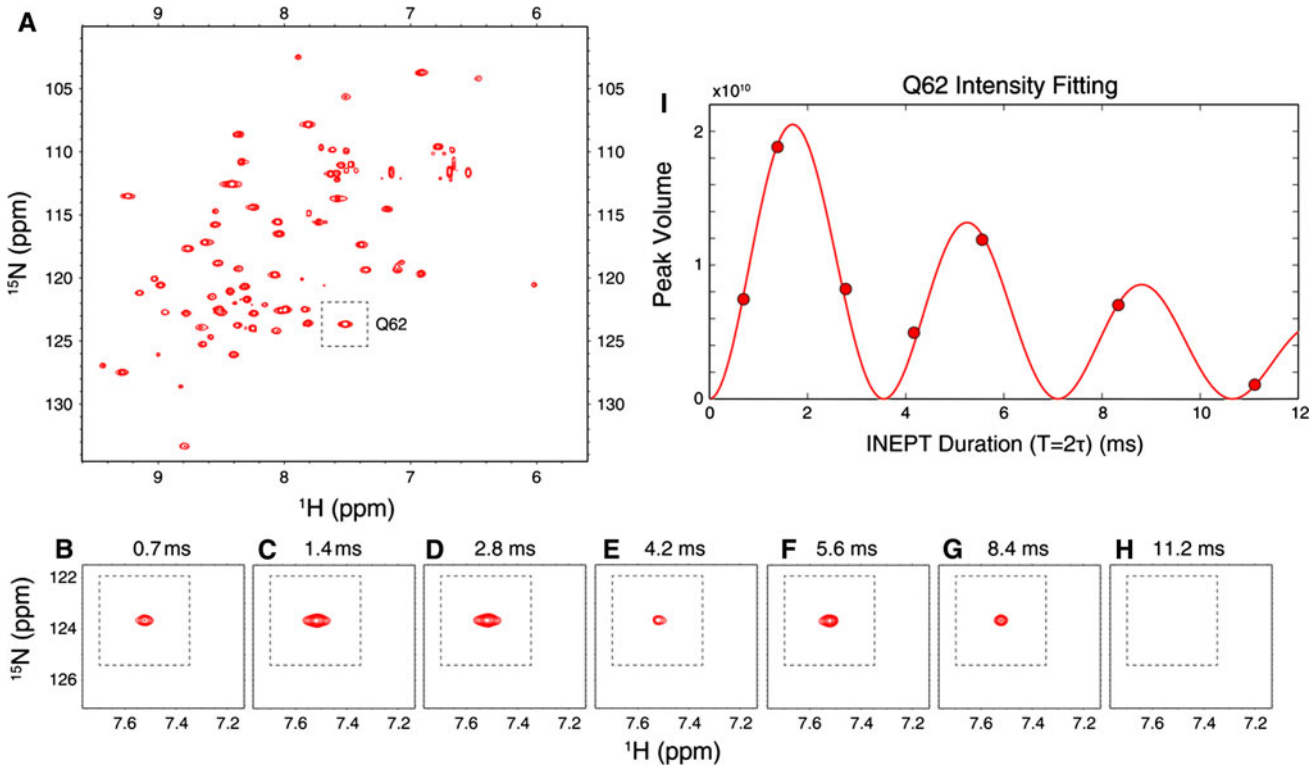

Fig. 3 (**a**) Overlay of the seven 2D spectra from the *J*-modulated ^{1}H–^{15}N HSQC series. One contour per spectrum is shown; negative contours are omitted (mainly sinc wiggles at the bottom of the strong peaks). The peak enclosed in a dashed-line box represents the correlation from residue Q62. (**b–h**) Spectral region containing the peak Q62 as extracted from the seven HSQC maps with different $T = 2\tau$ settings (the values of T are indicated above the panels). (**i**) Intensity (volume) of the peak Q62 plotted as a function of INEPT delay $T = 2\tau$. The curve displays the result of fitting using Eq. 2 with three floating parameters: intensity scaling factor I_0, spin coupling $|\Sigma|$ (fitted to 281.4 Hz), and effective decay rate of the transverse proton magnetization $R_{2,eff}$ (fitted to 50.1 s^{-1})

peak. At the same time anti-trosy component assumes the position that is normally associated with trosy. Fortunately, one can discriminate between these two scenarios based on the width of the respective resonances. For instance, in the case of Q62 the sharp peak in the lower right corner clearly represents the trosy component, whereas its broad counterpart in the upper left corner is anti-trosy (Fig. 4, panels (b–h)). This observation leads us to conclude that the net coupling Σ for residue Q62 is negative. Similar analyses, relying on quantitative peak widths of trosy, anti-trosy and HSQC correlations, allowed us to determine the sign of $\Sigma = {}^{1}J_{NH} + {}^{1}D_{NH}$ for other residues. While most of Σ values were found to be negative, a significant number turned out to be positive (corresponding to positive and large ${}^{1}D_{NH}$). Hence, the linewidth-based approach proves to be crucial for successful measurement of strong dipolar couplings.

Along with trosy and anti-trosy peaks, Figs. 4b–h also display two other components of the TROSY quartet (weak signals in the lower left and upper right corner of the dashed-line box). The intensities of all four components have been extracted using the *autofit* routine and then fitted to the theoretical dependencies from Tab. S1. The outcome of the fitting is shown in Figs. 4i–l, where the individual components of the quartet are identified by small diagrams to the right of the plot. Of note, the fitting procedure, which covers all four components of the quartet, employs only three variable parameters: overall intensity scaling factor I_0, the effective transverse relaxation rate $R_{2,eff}$, and the net coupling Σ. For the latter parameter the fitting led to $|\Sigma| = 287.1$ Hz, in good agreement with the previously derived values, 291.8 and 281.4 Hz.

The quality of the fit in Figs. 4i–l is not quite as good as in Fig. 3i. This can be understood considering that: (1) the fitting Fig. 4 involves four times as many experimental points, but the same number of adjustable parameters as in Fig. 3; (2) while HSQC peak appears in six spectral planes out of seven, trosy peak is present only in four disjointed planes, Figs. 4b–d, g, and anti-trosy in two planes, Figs. 4e, f, which affects the performance of *autofit*; (3) modeling of relaxation effects during the TROSY sequence remains relatively crude, see Tab. S1. Given all these limitations, the TROSY-based intensity fit in Figs. 4i–l appears reasonably successful. We have not

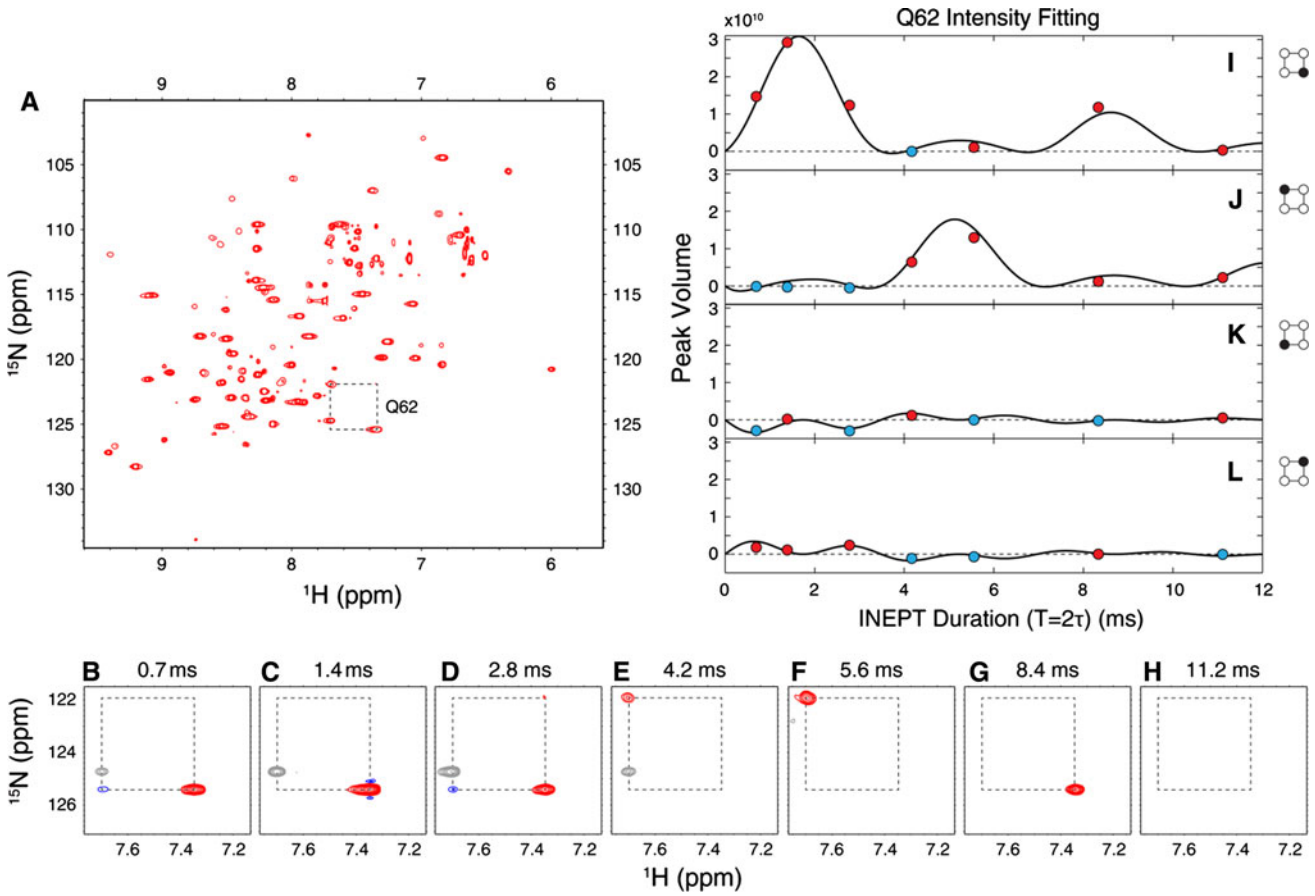

Fig. 4 (**a**) Overlay of the seven 2D spectra from the *J*-modulated ^{1}H–^{15}N TROSY series. One contour per spectrum is shown; negative contours are omitted. (**b–h**) Spectral region containing the signals from residue Q62 as extracted from the seven TROSY maps with different $T = 2\tau$ settings (the values of T are listed above the panels). The vertices of the dashed-line square indicate the location of the TROSY quartet from residue Q62 (reproduced from the panel (**a**)); the unrelated peak from residue D58 is colored grey. (**i–l**) Intensities (volumes) of the four components of the TROSY quartet from residue Q62 plotted as a function of INEPT delay $T = 2\tau$. Each component is identified by a diagram to the right of the respective panel. Positive (negative) intensities are represented by red (blue) circles. The data from all four components have been fitted simultaneously to the set of formulas in Tab. S1 with three global fitting parameters: overall intensity scaling factor I_0, spin coupling $|\Sigma|$ (fitted to 287.1 Hz), and effective decay rate of the transverse magnetization $R_{2,eff}$ (fitted to 64.2 s^{-1})

attempted, however, to extend this treatment beyond residue Q62 since we feel that HSQC-based intensity fit, Fig. 3i, is better suited for quantitation of $|\Sigma|$.

Figures 4b–h and 4i–l demonstrate another important property of the TROSY experiment with variable τ. Two minor components of the TROSY quartet are very weak—in fact, for all but a handful of residues these peaks fall under the noise level. On the other hand, trosy and anti-trosy peaks appear on an alternating basis—in other words, any chosen spectral plane contains either trosy or anti-trosy correlation from a given residue, but not both. Furthermore, one of these components tends to be weak as well. *In fact, for most residues the TROSY quartet is represented by a single observable peak. This peak is located below and to the right of the HSQC resonance and corresponds to either trosy or anti-trosy correlation (depending on the sign of* Σ*).* This kind of behavior—involving one dominant peak—can be readily reproduced using formulas in Tab. S1 (see also Fig. 4). Importantly, it means that the spectra do not suffer from excessive crowding and thus can be used to extract spin couplings. Specifically, the signed values of Σ can be obtained from the frequency shifts between trosy (anti-trosy) and HSQC resonances.

Reproducibility of the RDC data

In the series of *J*-modulated ^{1}H–^{15}N HSQC spectra we have reliably identified 58 backbone resonances. In the *J*-modulated ^{1}H–^{15}N TROSY spectra we found pairs for all of these peaks except four (two of the TROSY correlations turned out to be extremely weak and two more were overlapped). Thus 54 peak pairs are available for

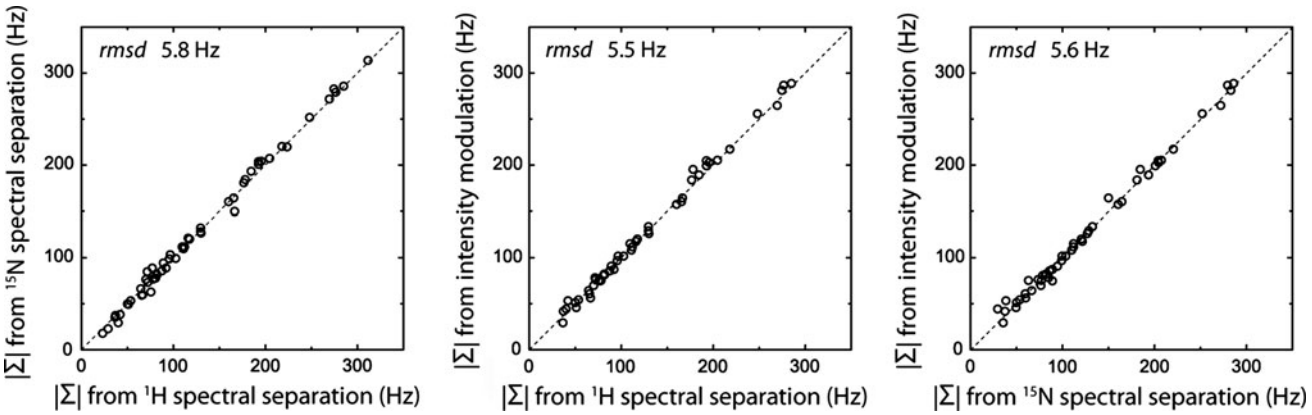

Fig. 5 Precision plots for $|\Sigma| = |{}^1J_{NH} + {}^1D_{NH}|$ data as measured from the intensity fitting or, alternatively, from the spectral separation between HSQC and TROSY peaks in either the ^{15}N or ^{1}H dimension

determination of $|\Sigma|$ based on the frequency separations in ^{15}N and ^{1}H dimensions. Note that at this stage we do not discriminate between trosy and anti-trosy correlations and therefore limit ourselves to the absolute value of Σ.

In addition, $|\Sigma|$ can be determined from modulation of the peak intensities in the HSQC spectra (cf. Fig. 3). Of 58 identifiable HSQC resonances, we have excluded two overlapped peaks as well as three peaks with poor *autofit* statistics (CHI2 > 0.1). The data from the remaining 53 peaks have been fitted to Eq. 2, producing a series of remarkably good fits (Fig. S6) and yielding the set of $|\Sigma|$ values.

In Fig. 5 we present the correlation plots for three $|\Sigma|$ datasets—two derived from ^{15}N and ^{1}H frequency separations between the TROSY and HSQC peaks and the third obtained from the intensity modulation of HSQC peaks. The agreement between all three datasets is good, as evidenced by *rmsd* of 5–6 Hz. Given that degree of alignment in our study is 10 times higher than usual (see below), this level of uncertainty corresponds to ca. 0.5 Hz error in the case of conventional measurements. Note that upward scaling of RDCs practically eliminates the effect of systematic measurement errors arising from unresolved scalar couplings and cross-correlated relaxation (de Alba and Tjandra 2006; Yao et al. 2009).

Structural analysis

Of 54 HSQC/TROSY peak pairs (Fig. 5a), only 44 have been confidently assigned. The remaining 10 signals could not be unambiguously identified. This situation is partially due to large residual CSA (RCSA) shifts—in our strongly aligned sample, RCSA shifts are estimated to reach 1 ppm in ^{15}N dimension and 0.05 ppm in ^{1}H^N dimension (Yao et al. 2010b, a). This obviously complicates the assignment transfer in the crowded regions of the spectrum. The fact that a number of correlations are missing (discussed below) creates additional difficulties. Note that in principle it is possible to back-calculate RCSA shifts and use this information to obtain additional assignments. However, as already stated, we prefer to avoid any possible circular reasoning and therefore do not employ RCSA or RDC data in the context of spectral assignment.

Of the 44 assigned HSQC/TROSY pairs, we have excluded terminal residues 73–76. These residue are highly mobile and thus unsuitable for the purpose of structural analyses (order parameter $S^2 = 0.57$ for residue L73 (Tjandra et al. 1995)). The remaining 40 pairs have been used to extract the RDC values ${}^1D_{NH}$. In the TROSY spectrum, we have initially focused on the peaks located below and to the right of the HSQC resonances (see previous discussion). The ^{15}N linewidths of these peaks, extracted with the help of *autofit*, have been compared with ^{15}N linewidths of the respective HSQC signals. Based on this comparison, the peaks were classified as trosy (sharper than HSQC, 28 instances) or anti-trosy (broader than HSQC, 12 instances). Accordingly, the decision was made on the sign of Σ: when the peak of interest was identified as trosy, the coupling Σ was deemed to be negative and the RDC constant was determined as ${}^1D_{NH} = -|\Sigma| - {}^1J_{NH}$; conversely, when the peak of interest was identified as anti-trosy, the coupling Σ was taken to be positive and the RDC constant was calculated as ${}^1D_{NH} = |\Sigma| - {}^1J_{NH}$.

As indicated above, we have focused on one TROSY component—specifically, the lower right peak in the ^{1}H^N–^{15}N quartet. Additionally, for 7 residues we have also captured the upper left peak. In each of these cases the analysis of ^{15}N linewidths confirmed our identification of the trosy and anti-trosy signals. It is worth noting that ^{15}N linewidths have been extracted from the spectra processed with the use of window function in nitrogen dimension (squared sine-bell). We found that the application of

window function does not change the *relative* amount of broadening in the HSQC and TROSY spectra.[3]

Note that ^{15}N dimension is better suited for the purpose of linewidth analysis than ^{1}H dimension. Indeed, for small globular proteins at room temperature the ^{15}N(CSA)–NH(dipole) cross-correlation rates are on average ca. twofold larger than ^{1}H(CSA)–NH(dipole) rates (Yao et al. 2010a, b).[4] Furthermore, ^{1}H(CSA)–NH(dipole) rates are highly variable—for some residues the effect all but disappears (Yao et al. 2010a). Finally, the intrinsic peak widths in ^{1}H dimension are significantly larger than in ^{15}N dimension (by 30 % in our measurements), which further complicates the detection of differential line broadening on protons. The analysis of our experimental data showed that in most cases ^{1}H linewidths are consistent with ^{15}N linewidths. However, in as many as 12 residues trosy peaks proved to be slightly broader in proton dimension than their HSQC counterparts (on average by less than 2 Hz). At least in part, this situation is certainly caused by noise. Under these circumstances, we choose to ignore the ^{1}H line broadening information.

In the end, our dataset was comprised of 40 signed $^{1}D_{NH}$ couplings. For each coupling, three values were available—two derived from ^{1}H and ^{15}N peak separations and one from the intensity fitting (see Fig. 5). For the purpose of structural analyses, these three values were averaged on per-residue basis (listed in Tab. S2). The results were then fitted to crystallographic structure 1UBQ, which provides a convenient benchmark for comparison to many RDC studies. The outcome of the fitting is illustrated in Fig. 6.

The quality factor of the fit in Fig. 6 is $Q = 0.160$. This is somewhat better than the range of Q that is normally obtained for crystal structures with ca. 1.8 Å resolution, $Q \approx 0.20 - 0.25$ (Bax 2003). This kind of agreement immediately suggests that our $^{1}D_{NH}$ data are not only precise but also accurate and, in particular, validates the sign determination procedure based on ^{15}N linewidths. The degree of alignment obtained from the fit in Fig. 6 is $A_a = -1.03 \times 10^{-2}$, which is an order of magnitude larger than typically encountered in weakly oriented samples.[5]

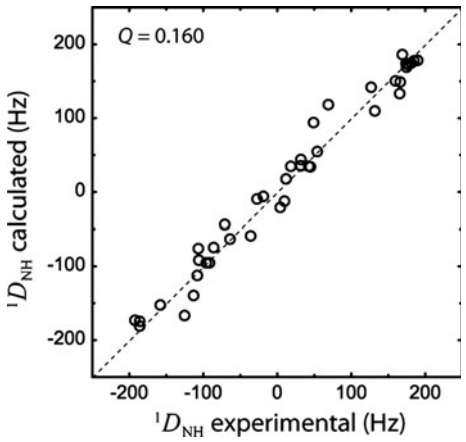

Fig. 6 Fitting of the experimental $^{1}D_{NH}$ data with crystallographic coordinates 1UBQ. Quality factor Q (Cornilescu et al. 1998) is 0.160. Slightly better quality factor, 0.152, can be obtained by (1) using the data derived from HSQC/TROSY nitrogen frequency separations alone and (2) applying a local-motion correction based on relaxation order parameters S

It is instructive to compare the results with the previously published data on ubiquitin in Pf1 media. Such comparison is presented in Table 2. Of particular interest is the RDC dataset reported by Briggman and Tolman (first row in Table 2). The Pf1 concentration employed in their study is much lower than in our work (3.5 mg/ml vs. 20 mg/ml), whereas the ionic strength of the solution is approximately similar (Briggman and Tolman 2003). As it turns out, the RDC constants reported by Briggman show an almost perfect correlation with our data, $r = 0.991$. At the same time the value of A_a in our experiment is 35 times higher than in Briggman's measurements. Taken together, these observations mean that the alignment in Pf1 media is highly scalable. In retrospect, this result is not surprising. The structure of charged, rod-shaped Pf1 particles is uniquely defined.[6] The interaction of ubiquitin with such particles is also a given. In this situation, the scaling of RDCs with phage concentration represents a relatively straightforward concentration effect. The risk of structural distortions due to Pf1-protein interactions is no different for high-concentration and low-concentration Pf1 media.

Of note, salting the sample does not have quite the same effect as varying the concentration of Pf1. While salt has a general screening effect leading to decreases in A_a, it may also alter the pattern of electrostatic interactions (Zweckstetter et al. 2004). This is a likely reason why our results do not agree quite as well with the data of Lakomek et al., $r = 0.941$ (middle row in Table 2).

[3] The difference between ^{15}N linewidths of the HSQC and TROSY signals is modest—for most residues it does not exceed 5 Hz. Because cross-correlated relaxation rates in ubiquitin are relatively small, the experiments that rely on cross-correlated relaxation transfer such as CRINEPT (Riek et al. 1999) do not perform well. This fact—which has been verified experimentally—underscores the difference between the current situation and the spectroscopy of large proteins in solution.

[4] Keep in mind, however, that the difference between HSQC and TROSY linewidths is not limited to CSA-dipolar cross-correlation, but also includes a small term originating from dipolar NH auto-relaxation.

[5] The generalized degree of order is 1.11×10^{-2} (Tolman et al. 2001).

[6] Although certain details may vary, e.g. phage particles may form dimers or higher order multimers in a concentration-dependent manner (Zweckstetter and Bax 2001).

Table 2 Summary of the literature results on ^{1}H-^{15}N RDCs of ubiquitin in Pf1 media

Reference	Sample conditions	Number of $^{1}D_{NH}$ RDCs available for comparison with our data	A_a from fitting with 1UBQ	Q from fitting with 1UBQ	Correlation with our RDC data r
(Briggman and Tolman 2003)	3.5 mg/ml Pf1 20 mM NaCl pH 6.6 308 K	37	-2.96×10^{-4}	0.154	0.991
(Lakomek et al. 2006) *Dataset E5*	15 mg/ml Pf1 400 mM NaCl pH 6.5 308 K	28	-8.53×10^{-4}	0.149	0.941
(Lakomek et al. 2006) *Dataset D5*	17 mg/ml Pf1 350 mM NaCl pH 6.5 308 K	11[a]	-2.39×10^{-3}	0.223	0.986

The original datasets have been trimmed so that they include only those residues that are also found in our dataset (column 3). These reduced datasets have been fitted with the structure 1UBQ (columns 4 and 5) and also correlated directly with the RDC data from this work (column 6). The complete alignment tensors can be found in Tab. S3

[a] The total of only 23 proton-nitrogen RDCs have been collected from this protonated sample which displays a relatively substantial degree of alignment

Completeness of the data

As already indicated, we have reliably identified 58 out of 73 potentially observable backbone amide resonances and assigned 44 of them. What is the issue with the missing peaks? Correlations from E24 and G53 were absent from all spectra (including isotropic samples) due to exchange broadening caused by a variable hydrogen bond between these two residues (Sidhu et al. 2011). Among 13 other missing peaks, a few are probably missed due to overlaps. Given that some of the peaks are rather weak, we may not be able to recognize them as overlaps if they are masked by stronger signals. Others are likely unobservable due to small net couplings. Among the couplings that we successfully measured there are none with $|\Sigma|$ less than 25 Hz (the weakest coupling that we have measured is $\Sigma = -26$ Hz in V70; incidentally, it is a very weak peak, which is also the worst outlier in the structural fit Fig. 6). Obviously, we fail to detect the signals with low $|\Sigma|$ because this requires very long INEPT delays, during which the signal decays away. For instance, when the HSQC experiment is tuned to $\Sigma_0 = 22.5$ Hz, the net length of INEPT evolution amounts to 66.6 ms. Most of this time the magnetization is transverse (cf. Eq. 2). Not surprisingly, the spectrum acquired with these settings was devoid of any significant signal (data not shown).

The detailed analysis of the missing resonances presents a certain difficulty because the spectral assignment is incomplete (i.e. much of the time we cannot tell whether the peak is truly missing or simply remains unassigned). Only in two cases we can confidently say that the peaks are actually missing—these are K33 and T55. A back-calculation using the alignment parameters obtained in the previous section, cf. Fig. 6, confirms that both K33 and T55 should exhibit relatively small couplings $|\Sigma|$. Furthermore, inspecting the list of back-calculated couplings we discover five other residues with $|\Sigma| < 25$ Hz that are either unobservable or possibly unassigned in our spectra.

Finally, it remains to discuss the cause of magnetization losses that occur during the INEPT periods and, more generally, during the course of the pulse sequences. Under low ionic strength conditions, the interaction between ubiquitin and Pf1 can be described as *transient binding*; the residence time for ubiquitin on the surface of Pf1 is $\tau_{res} = 1/k_{off}$. For the sake of discussion let us focus on an isolated ^{15}N,^{1}H^{N} pair in ubiquitin. When ubiquitin is bound to the phage, the dipolar coupling between these two spins is large (d_{NH} up to 10 kHz, depending on the orientation of the N-H^{N} bond relative to the director of Pf1 media). On the other hand, in the free state of ubiquitin this coupling drops to zero. Hence, ^{15}N spin experiences the effect of time-variable dipolar interaction which is modulated by on–off exchange between the free and bound states. Given that the free form dominates, it is easy to show that the characteristic exchange time is determined by the off-rate, $\tau_{ex} \approx \tau_{res} = 1/k_{off}$.

Assuming that exchange is fast on the scale of dipolar interaction strength, i.e. $d_{NH}\tau_{ex} \ll 1$, this situation can be described by means of the Redfield theory. Proceeding along the same lines as in the case of scalar relaxation of the first kind (Abragam 1961), one can predict the amount of ^{15}N line-broadening resulting from on–off exchange:

$$R_2^{dip,exch}(^{15}\mathrm{N}) = p_{free}p_{bound}(2\pi d_{NH})^2\tau_{ex} \quad (3)$$

where p_{free} and p_{bound} is the fraction of free and bound ubiquitin, respectively. Based on the determined degree of alignment A_a, we can estimate that ca. 1 % of ubiquitin in our sample is in the bound form. Assuming further that the residence time of ubiquitin on the surface of Pf1 is 1 μs, we can calculate the $R_2^{dip,exch}$ contribution into ^{15}N relaxation, which amounts up to 40 s^{-1}. In the case of ^{1}H^{N} transverse

magnetization the effect is expected to be even more pronounced since $^{1}H^{N}$ is also affected by proton–proton interactions (including protons at the exchangeable sites in ubiquitin, as well as Pf1 protons). These estimates are consistent with our experimental observations and, in particular, with $R_{2,eff}$ values $\sim 50\ s^{-1}$ obtained in the *J*-modulated experiments (see Fig. 3).

It is also instructive to discuss what happens if the residence time τ_{res} increases toward 100 μs (i.e. in the case of relatively strong binding). This situation will have a number of consequences. The broadening of spectral lines will become dramatic. Indeed, the system will approach the coalescence point (where Redfield-type treatment breaks down). The entire concept of RDCs will become meaningless. Instead, one would have to consider the evolution of the spin system which exchanges between the two states, one of which is classified as solid and the other as a solution. Note that dissipation of spin magnetization in the solid state is especially dramatic because of proton spin diffusion that cannot be properly refocused. The fact that we do not observe this catastrophic scenario indicates that τ_{res} remains relatively short (Zweckstetter et al. 2004).

The losses of proton magnetization are also important in the context of possible $^{1}H^{N}$–$^{1}H^{N}$ COSY-type experiments. The key parameter which determines the success of such measurements is the ratio $|^{1}D_{NH}|_{\max}/R_{2,eff}$, which in our case reaches ca. 3.0. This is similar or possibly somewhat better than what can be achieved for small deuterated proteins in weakly orienting media. Therefore our strongly aligned sample should be suitable for measuring long proton–proton distances similar to the previously reported applications (Tian et al. 2000; Wu and Bax 2002; Meier et al. 2003; Schanda et al. 2007).

Concluding remarks

The majority of popular alignment media do not have perfect scaling properties. When DHPC/DMPC media is prepared using a high phospholipid concentration, it forms a stable nematic phase which can tolerate a wide range of perturbations (Sanders and Schwonek 1992; Harroun et al. 2005). However, when the media is diluted toward the concentration typically used in protein NMR (approx. 5 % w/v) its properties begin to deteriorate—the temperature range narrows, the molar ratio DMPC:DHPC becomes more restrictive, the sample tends to undergo phase separation, etc. (Ottiger and Bax 1998; Losonczi and Prestegard 1998; Harroun et al. 2005). Finally, below the threshold concentration of ca. 3 % w/v the nematic phase disappears altogether. Other popular liquid crystal media, such as Pf1 phage and PEG/hexanol, suffer from the same predicament (Zweckstetter and Bax 2001; Jonstromer and Strey 1992).

In view of these observations, one may speculate that other liquid crystal media exist that are potentially suitable for protein work (Chernik 1999), but currently remain unused because they do not respond well to dilution. In this study we seek to expand the boundaries of what is considered a "dilute alignment media". Specifically, we demonstrate that a media with a relatively high degree of alignment, $A_a \sim 10^{-2}$, can be used to successfully measure $^{1}H^{N}$–^{15}N RDCs by means of solution-state spectroscopy. These measurements require a protein sample with a high level of deuteration. Although deuterated samples remain relatively expensive, they are routinely used in biomolecular NMR—the deuterated protein material is often at hand during the course of structural studies. The ^{2}H decoupling capabilities, which are also required in our experiments, are commonly available as well.

The relatively high degree of alignment obtained in our study gives rise to $^{1}H^{N}$–^{15}N RDCs in the range from −200 to 200 Hz. This is an order of magnitude larger than typically attainable in solution. Such a broad range of couplings cannot be measured using standard experimental schemes that employ fixed-delay INEPT elements. To address this problem we have implemented several *J*-resolved and *J*-modulated experiments which are suitable for a broad distribution of RDC values. The signs of the couplings are determined based on identification of the trosy/anti-trosy components in the $^{1}H^{N}$–^{15}N quartet. These components can no longer be identified based on the usual spectral pattern—instead, we rely on ^{15}N linewidth.

It is worth noting that ^{15}N(CSA)–NH(dipole) cross-correlations in ubiquitin are relatively small—yet sufficient to reliably identify the trosy/anti-trosy peaks. For bigger-size proteins this identification should be easier. Generally, the described experiments should perform well for mid-sized proteins. Indeed, the usual relaxation losses which involve a protein freely tumbling in solution do not present a bottleneck in the context of our measurements. The main mechanism of magnetization losses is different and has to do with transient interactions between the protein and the alignment media. Therefore it should be possible to study a protein twice the size of ubiquitin without significantly affecting the quality of spectral signals. Similar to solid-state spectroscopy, the utility of this approach may be limited by crowding of the spectral map and difficulties in assigning the signals. These observations put in a spotlight the dual nature of our experimental system where the protein exchanges between the solution- and solid-like situations (free and bound states). This kind of duality is expected to give rise to interesting spin dynamics, which awaits further investigation.

Acknowledgments We thank Konstantin Pervushin for bringing to our attention the problem of exchange between solution- and solid-

like environments. We would also like to acknowledge Nils-Alexander Lakomek and Korvin Walter who provided to us their spectral assignment data. We are thankful to Lewis Kay and Yi Xue for critical reading of the manuscript. This work was supported by NSF awards MCB 0445643 and 105814.

References

Abragam A (1961) The principles of nuclear magnetism. Clarendon Press, Oxford

Agarwal V, Reif B (2008) Residual methyl protonation in perdeuterated proteins for multi-dimensional correlation experiments in MAS solid-state NMR spectroscopy. J Magn Reson 194:16–24

Akbey U, Lange S, Franks WT, Linser R, Rehbein K, Diehl A, van Rossum BJ, Reif B, Oschkinat H (2010) Optimum levels of exchangeable protons in perdeuterated proteins for proton detection in MAS solid-state NMR spectroscopy. J Biomol NMR 46:67–73

Bax A (2003) Weak alignment offers new NMR opportunities to study protein structure and dynamics. Protein Sci 12:1–16

Briggman KB, Tolman JR (2003) De Novo determination of bond orientations and order parameters from residual dipolar couplings with high accuracy. J Am Chem Soc 125:10164–10165

Brooks BR, Brooks CL, Mackerell AD, Nilsson L, Petrella RJ, Roux B, Won Y, Archontis G, Bartels C, Boresch S, Caflisch A, Caves L, Cui Q, Dinner AR, Feig M, Fischer S, Gao J, Hodoscek M, Im W, Kuczera K, Lazaridis T, Ma J, Ovchinnikov V, Paci E, Pastor RW, Post CB, Pu JZ, Schaefer M, Tidor B, Venable RM, Woodcock HL, Wu X, Yang W, York DM, Karplus M (2009) CHARMM: the biomolecular simulation program. J Comput Chem 30:1545–1614

Brunger AT (1992) X-PLOR, version 3.1. A system for X-ray crystallography and NMR. Yale University Press, New Haven

Cai S, Seu C, Kovacs Z, Sherry AD, Chen Y (2006) Sensitivity enhancement of multidimensional NMR experiments by paramagnetic relaxation effects. J Am Chem Soc 128:13474–13478

Cavanagh J, Fairbrother WJ, Palmer AG, Skelton NJ, Rance M (2007) Protein NMR spectroscopy. Principles and practice, 2nd edn. Academic Press Inc., San Diego

Chen ZJ, Krause G, Reif B (2005) Structure and orientation of peptide inhibitors bound to beta-amyloid fibrils. J Mol Biol 354:760–776

Chernik GG (1999) Phase studies of surfactant-water systems. Curr Opin Colloid Interface Sci 4:381–390

Chevelkov V, Rehbein K, Diehl A, Reif B (2006) Ultra-high resolution in proton solid-state NMR spectroscopy at high levels of deuteration. Angew Chem Int Ed 45:3878–3881

Chevelkov V, Fink U, Reif B (2009) Accurate determination of order parameters from ^{1}H,^{15}N dipolar couplings in MAS solid-state NMR experiments. J Am Chem Soc 131:14018–14022

Cornilescu G, Marquardt JL, Ottiger M, Bax A (1998) Validation of protein structure from anisotropic carbonyl chemical shifts in a dilute liquid crystalline phase. J Am Chem Soc 120:6836–6837

de Alba E, Tjandra N (2006) On the accurate measurement of amide one-bond ^{15}N–^{1}H couplings in proteins: effects of cross-correlated relaxation, selective pulses and dynamic frequency shifts. J Magn Reson 183:160–165

Delaglio F, Grzesiek S, Vuister GW, Zhu G, Pfeifer J, Bax A (1995) NMRPipe—a multidimensional spectral processing system based on unix pipes. J Biomol NMR 6:277–293

Eletsky A, Moreira O, Kovacs H, Pervushin K (2003) A novel strategy for the assignment of side-chain resonances in completely deuterated large proteins using ^{13}C spectroscopy. J Biomol NMR 26:167–179

Emsley JW, Lindon JC (1975) NMR spectroscopy using liquid crystal solvents. Pergamon Press, Oxford

Furihata K, Seto H (1999) J-resolved HMBC, a new NMR technique for measuring heteronuclear long-range coupling constants. Tetrahedron Lett 40:6271–6275

Furrer J, John M, Kessler H, Luy B (2007) J-Spectroscopy in the presence of residual dipolar couplings: determination of one-bond coupling constants and scalable resolution. J Biomol NMR 37:231–243

Gardner KH, Kay LE (1998) The use of ^{2}H, ^{13}C, ^{15}N multidimensional NMR to study the structure and dynamics of proteins. Annu Rev Biophys Biomol Struct 27:357–406

Goto NK, Gardner KH, Mueller GA, Willis RC, Kay LE (1999) A robust and cost-effective method for the production of Val, Leu, Ile-δ1 methyl-protonated ^{15}N, ^{13}C, ^{2}H-labeled proteins. J Biomol NMR 13:369–374

Hansen MR, Mueller L, Pardi A (1998) Tunable alignment of macromolecules by filamentous phage yields dipolar coupling interactions. Nat Struct Biol 5:1065–1074

Harroun TA, Koslowsky M, Nieh MP, de Lannoy CF, Raghunathan VA, Katsaras J (2005) Comprehensive examination of mesophases formed by DMPC and DHPC mixtures. Langmuir 21:5356–5361

Hewitt RC, Meiboom S, Snyder LC (1973) Proton NMR in nematic liquid crystalline solvents: use of deuterium decoupling. J Chem Phys 58:5089–5095

Hohwy M, Jaroniec CP, Reif B, Rienstra CM, Griffin RG (2000) Local structure and relaxation in solid-state NMR: accurate measurement of amide N-H bond lengths and H-N-H bond angles. J Am Chem Soc 122:3218–3219

Hus JC, Prompers JJ, Bruschweiler R (2002) Assignment strategy for proteins with known structure. J Magn Reson 157:119–123

Jensen P, Sass HJ, Grzesiek S (2004) Improved detection of long-range residual dipolar couplings in weakly aligned samples by Lee-Goldburg decoupling of homonuclear dipolar truncation. J Biomol NMR 30:443–450

Jonstromer M, Strey R (1992) Nonionic bilayers in dilute solutions: effect of additives. J Phys Chem 96:5993–6000

Kay LE, Keifer P, Saarinen T (1992) Pure absorption gradient enhanced heteronuclear single quantum correlation spectroscopy with improved sensitivity. J Am Chem Soc 114:10663–10665

Kelly GP, Muskett FW, Whitford D (1996) 3D J-resolved HSQC, a novel approach to measuring $^{3}J_{HN\alpha}$. Application to paramagnetic proteins. J Magn Reson Ser B 113:88–90

Kishore AI, Prestegard JH (2003) Molecular orientation and conformation of phosphatidylinositides in membrane mimetics using variable angle sample spinning (VASS) NMR. Biophys J 85: 3848–3857

Koenig BW, Kontaxis G, Mitchell DC, Louis JM, Litman BJ, Bax A (2002) Structure and orientation of a G protein fragment in the receptor bound state from residual dipolar couplings. J Mol Biol 322:441–461

Kontaxis G, Clore GM, Bax A (2000) Evaluation of cross-correlation effects and measurement of one-bond couplings in proteins with short transverse relaxation times. J Magn Reson 143:184–196

Koradi R, Billeter M, Wüthrich K (1996) MOLMOL: a program for display and analysis of macromolecular structures. J Mol Graph 14:51–55

Lakomek NA, Carlomagno T, Becker S, Griesinger C, Meiler J (2006) A thorough dynamic interpretation of residual dipolar couplings in ubiquitin. J Biomol NMR 34:101–115

Lancelot N, Elbayed K, Piotto M (2005) Applications of variable-angle sample spinning experiments to the measurement of scaled residual dipolar couplings and ^{15}N CSA in soluble proteins. J Biomol NMR 33:153–161

Lazar GA, Desjarlais JR, Handel TM (1997) De novo design of the hydrophobic core of ubiquitin. Protein Sci 6:1167–1178

Levante TO, Bremi T, Ernst RR (1996) Pulse-sequence optimization with analytical derivatives. Application to deuterium decoupling in oriented phases. J Magn Reson Ser A 121:167–177

Levitt MH (1997) The signs of frequencies and phases in NMR. J Magn Reson 126:164–182

Li MX, Corson DC, Sykes BD (2002) In: Vogel HJ (eds) Methods in molecular biology, vol 173, pp 255–265

Lichtenecker R, Ludwiczek ML, Schmid W, Konrat R (2004) Simplification of protein NOESY spectra using bioorganic precursor synthesis and NMR spectral editing. J Am Chem Soc 126:5348–5349

LiWang AC, Bax A (1996) Equilibrium protium/deuterium fractionation of backbone amides in U-^{13}C/^{15}N labeled human ubiquitin by triple resonance NMR. J Am Chem Soc 118:12864–12865

Losonczi JA, Prestegard JH (1998) Improved dilute bicelle solutions for high-resolution NMR of biological macromolecules. J Biomol NMR 12:447–451

Luy B, Marino JP (2003) JE-TROSY: combined J- and TROSY-spectroscopy for the measurement of one-bond couplings in macromolecules. J Magn Reson 163:92–98

Luy B, Kobzar K, Kessler H (2004) An easy and scalable method for the partial alignment of organic molecules for measuring residual dipolar couplings. Angew Chem Int Ed 43:1092–1094

Meier S, Haussinger D, Jensen P, Rogowski M, Grzesiek S (2003) High-accuracy residual $^{1}H^{N}$–^{13}C and $^{1}H^{N}$–$^{1}H^{N}$ dipolar couplings in perdeuterated proteins. J Am Chem Soc 125:44–45

Meier S, Strohmeier M, Blackledge M, Grzesiek S (2007) Direct observation of dipolar couplings and hydrogen bonds across a β-hairpin in 8 M urea. J Am Chem Soc 129:754–755

Nielsen NC, Bildsoe H, Jakobsen HJ, Sorensen OW (1989) Composite refocusing sequences and their application for sensitivity enhancement and multiplicity filtration in INEPT and 2D correlation spectroscopy. J Magn Reson 85:359–380

Nietlispach D (2005) Suppression of anti-TROSY lines in a sensitivity enhanced gradient selection TROSY scheme. J Biomol NMR 31:161–166

Nietlispach D, Clowes RT, Broadhurst RW, Ito Y, Keeler J, Kelly M, Ashurst J, Oschkinat H, Domaille PJ, Laue ED (1996) An approach to the structure determination of larger proteins using triple resonance NMR experiments in conjunction with random fractional deuteration. J Am Chem Soc 118:407–415

Ojennus DD, Mitton-Fry RM, Wuttke DS (1999) Induced alignment and measurement of dipolar couplings of an SH2 domain through direct binding with filamentous phage. J Biomol NMR 14:175–179

Ottiger M, Bax A (1998) Characterization of magnetically oriented phospholipid micelles for measurement of dipolar couplings in macromolecules. J Biomol NMR 12:361–372

Ottiger M, Delaglio F, Bax A (1998) Measurement of *J* and dipolar couplings from simplified two-dimensional NMR spectra. J Magn Reson 131:373–378

Pines A, Ruben DJ, Vega S, Mehring M (1976) New approach to high-resolution proton NMR in solids: deuterium spin decoupling by multiple-quantum transitions. Phys Rev Lett 36: 110–113

Prestegard JH, Kishore AI (2001) Partial alignment of biomolecules: an aid to NMR characterization. Curr Opin Chem Biol 5:584–590

Riek R, Wider G, Pervushin K, Wuthrich K (1999) Polarization transfer by cross-correlated relaxation in solution NMR with very large molecules. Proc Natl Acad Sci USA 96:4918–4923

Sanders CR, Schwonek JP (1992) Characterization of magnetically orientable bilayers in mixtures of dihexanoylphosphatidylcholine and dimyristoylphosphatidylcholine by solid-state NMR. Biochemistry 31:8898–8905

Schanda P, Lescop E, Falge M, Sounier R, Boisbouvier J, Brutscher B (2007) Sensitivity-optimized experiment for the measurement of residual dipolar couplings between amide protons. J Biomol NMR 38:47–55

Schenker KV, Suter D, Pines A (1987) Broadband heteronuclear decoupling in the presence of homonuclear dipolar and quadrupolar interactions. J Magn Reson 73:99–113

Schwieters CD, Kuszewski JJ, Tjandra N, Clore GM (2003) The Xplor-NIH NMR molecular structure determination package. J Magn Reson 160:65–73

Shaka AJ, Barker PB, Freeman R (1985) Computer-optimized decoupling scheme for wideband applications and low-level operation. J Magn Reson 64:547–552

Sidhu A, Surolia A, Robertson AD, Sundd M (2011) A hydrogen bond regulates slow motions in ubiquitin by modulating a ß-turn flip. J Mol Biol 411:1037–1048

Sounier R, Blanchard L, Wu ZR, Boisbouvier J (2007) High-accuracy distance measurement between remote methyls in specifically protonated proteins. J Am Chem Soc 129:472–473

Su XC, Otting G (2010) Paramagnetic labelling of proteins and oligonucleotides for NMR. J Biomol NMR 46:101–112

Thiele CM (2005) Scaling the alignment of small organic molecules in substituted polyglutamates by variable-angle sample spinning. Angew Chem Int Ed 44:2787–2790

Tian F, Losonczi JA, Fischer MWF, Prestegard JH (1999) Sign determination of dipolar couplings in field-oriented bicelles by variable angle sample spinning (VASS). J Biomol NMR 15:145–150

Tian F, Fowler CA, Zartler ER, Jenney FA, Adams MW, Prestegard JH (2000) Direct measurement of ^{1}H–^{1}H dipolar couplings in proteins: a complement to traditional NOE measurements. J Biomol NMR 18:23–31

Tjandra N, Bax A (1997) Direct measurement of distances and angles in biomolecules by NMR in a dilute liquid crystalline medium. Science 278:1111–1114

Tjandra N, Feller SE, Pastor RW, Bax A (1995) Rotational diffusion anisotropy of human ubiquitin from ^{15}N NMR relaxation. J Am Chem Soc 117:12562–12566

Tjandra N, Grzesiek S, Bax A (1996) Magnetic field dependence of nitrogen-proton J splittings in ^{15}N-enriched human ubiquitin resulting from relaxation interference and residual dipolar coupling. J Am Chem Soc 118:6264–6272

Tolman JR, Prestegard JH (1996) A quantitative J-correlation experiment for the accurate measurement of one-bond amide ^{15}N–^{1}H couplings in proteins. J Magn Reson Ser B 112: 245–252

Tolman JR, Ruan K (2006) NMR residual dipolar couplings as probes of biomolecular dynamics. Chem Rev 106:1720–1736

Tolman JR, Flanagan JM, Kennedy MA, Prestegard JH (1995) Nuclear magnetic dipole interactions in field-oriented proteins: information for structure determination in solution. Proc Natl Acad Sci USA 92:9279–9283

Tolman JR, Al-Hashimi HM, Kay LE, Prestegard JH (2001) Structural and dynamic analysis of residual dipolar coupling data for proteins. J Am Chem Soc 123:1416–1424

Torchia DA, Sparks SW, Bax A (1988) NMR signal assignments of amide protons in the α-helical domains of staphylococcal nuclease. Biochemistry 27:5135–5141

Trempe JF, Pomerantseva E, Gehring K (2008) REDOR recoupling in polymer-stabilized liquid crystals undergoing MAS—two-dimensional NMR applications with strongly aligned proteins. Can J Chem 86:608–615

Ulmer TS, Ramirez BE, Delaglio F, Bax A (2003) Evaluation of backbone proton positions and dynamics in a small protein by liquid crystal NMR spectroscopy. J Am Chem Soc 125: 9179–9191

Vander Kooi CW, Kupce E, Zuiderweg ERP, Pellecchia M (1999) Line narrowing in spectra of proteins dissolved in a dilute liquid

crystalline phase by band-selective adiabatic decoupling: application to $^{1}H^{N}$–^{15}N residual dipolar coupling measurements. J Biomol NMR 15:335–338

Veglia G, Gopinath T (2010) Improved resolution in dipolar NMR spectra using constant time evolution PISEMA experiment. Chem Phys Lett 494:104–110

Vijay-Kumar S, Bugg CE, Cook WJ (1987) Structure of ubiquitin refined at 1.8 Å resolution. J Mol Biol 194:531–544

Wang YX, Marquardt JL, Wingfield P, Stahl SJ, Lee-Huang S, Torchia D, Bax A (1998) Simultaneous measurement of ^{1}H–^{15}N, ^{1}H–$^{13}C'$, and ^{15}N–$^{13}C'$ dipolar couplings in a perdeuterated 30 kDa protein dissolved in a dilute liquid crystailine phase. J Am Chem Soc 120:7385–7386

Wu ZR, Bax A (2002) Measurement of long-range ^{1}H–^{1}H dipolar couplings in weakly aligned proteins. J Am Chem Soc 124: 9672–9673

Yao LS, Vögeli B, Ying JF, Bax A (2008) NMR determination of amide N-H equilibrium bond length from concerted dipolar coupling measurements. J Am Chem Soc 130:16518–16520

Yao LS, Ying JF, Bax A (2009) Improved accuracy of ^{15}N–^{1}H scalar and residual dipolar couplings from gradient-enhanced IPAP-HSQC experiments on protonated proteins. J Biomol NMR 43: 161–170

Yao LS, Grishaev A, Cornilescu G, Bax A (2010a) The impact of hydrogen bonding on amide ^{1}H Chemical Shift Anisotropy studied by cross-correlated relaxation and liquid crystal NMR spectroscopy. J Am Chem Soc 132:10866–10875

Yao LS, Grishaev A, Cornilescu G, Bax A (2010b) Site-specific backbone amide ^{15}N chemical shift anisotropy tensors in a small protein from liquid crystal and cross-correlated relaxation measurements. J Am Chem Soc 132:4295–4309

Yuwen T, Post CB, Skrynnikov NR (2011) Domain cooperativity in multidomain proteins: what can we learn from molecular alignment in anisotropic media? J Biomol NMR 51:131–150

Zandomeneghi G, Meier BH (2004) Adiabatic-passage cross polarization in ^{15}N NMR spectroscopy of peptides weakly associated to phospholipids: determination of large RDC. J Biomol NMR 30:303–309

Zandomeneghi G, Tomaselli M, Williamson PTF, Meier BH (2003) NMR of bicelles: orientation and mosaic spread of the liquid-crystal director under sample rotation. J Biomol NMR 25: 113–123

Zweckstetter M (2008) NMR: prediction of molecular alignment from structure using the PALES software. Nat Protoc 3:679–690

Zweckstetter M, Bax A (2001) Characterization of molecular alignment in aqueous suspensions of Pf1 bacteriophage. J Biomol NMR 20:365–377

Zweckstetter M, Hummer G, Bax A (2004) Prediction of charge-induced molecular alignment of biomolecules dissolved in dilute liquid-crystalline phases. Biophys J 86:3444–3460

Supplementary information:

Very large residual dipolar couplings from deuterated ubiquitin

Joshua M. Ward† and Nikolai R. Skrynnikov*

Department of Chemistry, Purdue University, 560 Oval Drive, West Lafayette, Indiana 47907-2084, USA

* E-mail: nikolai@purdue.edu

† Current address: Chemistry Department, University of Oulu, POB 3000, 90014 Oulu, Finland.

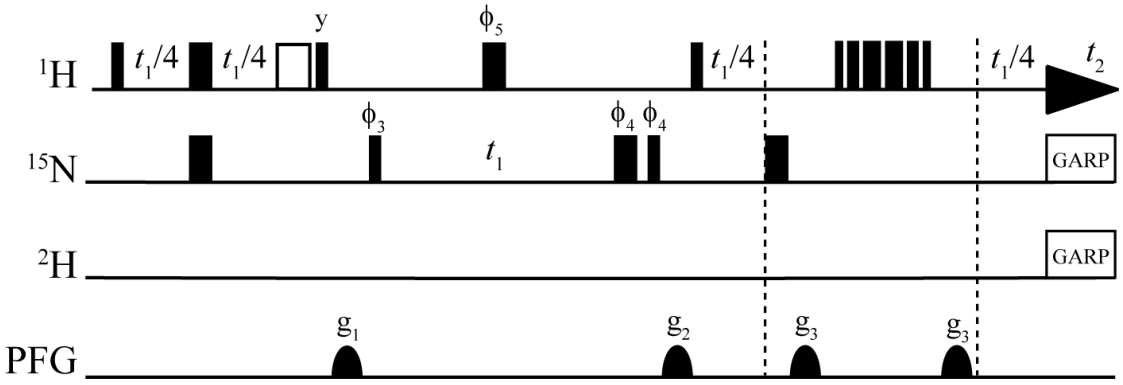

Figure S1: Pulse sequence diagram of the *J*-resolved ^{1}H,^{15}N HSQC experiment used to observe peak splittings from a broad range of couplings $\Sigma = {}^1J_{NH} + {}^1D_{NH}$ in a single 2D spectrum. The pulse shown with an open rectangle is a high-power 1-ms trim pulse. The WATERGATE solvent suppression scheme utilizes 3-9-19 composite proton pulse with the standard phase settings [Sklenar *et al.* J. Magn. Reson. A **102**, 241]. The phase cycle is ϕ_3=(x,–x), ϕ_4=4(x)4(–x), ϕ_5=2(x)2(–x), rec=(x,–x, x,–x,–x, x,–x, x). ^{15}N and ^{2}H decoupling during the 80-ms acquisition period is applied with *rf* field strength of 1.3 and 1.1 kHz, respectively. The gradients are $g1 = (40\ \text{G/cm}, 1\ \text{ms})$, $g2 = (-25\ \text{G/cm}, 1\ \text{ms})$, and $g3 = (15\ \text{G/cm}, 1\ \text{ms})$.

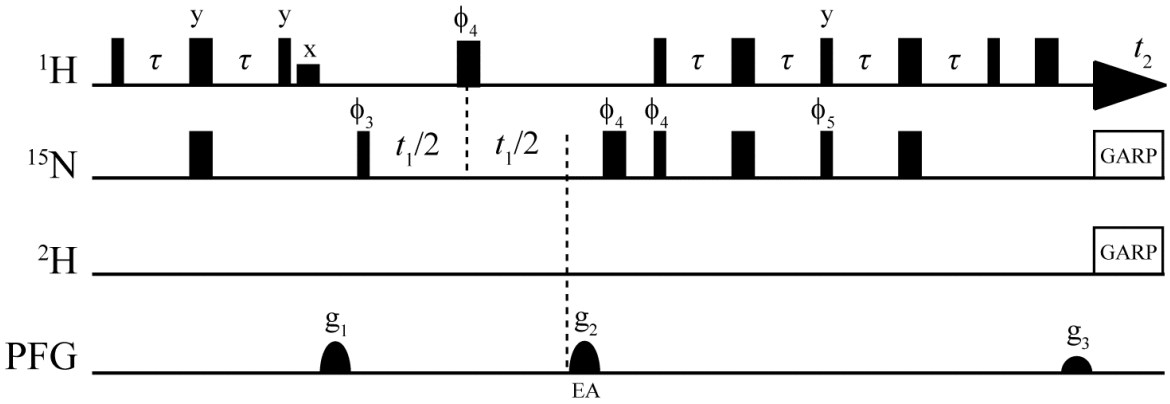

Figure S2: Pulse sequence diagram of the ^{1}H,^{15}N HSQC experiment with variable INEPT delays τ. The pulse shown with a small solid rectangle is 90° sinc-shaped water flip-back pulse (duration 1 ms). The phase cycle is ϕ_3=(x,–x), ϕ_4=2(x)2(–x), ϕ_5=2(y)2(–y), rec=(x,–x,–x, x). ^{15}N and ^{2}H decoupling during the 80-ms acquisition period is applied with *rf* field strength of 1.3 and 1.1 kHz, respectively. The echo-antiecho gradient selection scheme is standard [Kay *et al.* J. Am. Chem. Soc. **114**, 10663]. The gradients are $g1 = (25\ \text{G/cm}, 1\ \text{ms})$, $g2 = (\pm 40\ \text{G/cm}, 1\ \text{ms})$, and $g3 = (4.05\ \text{G/cm}, 1\ \text{ms})$.

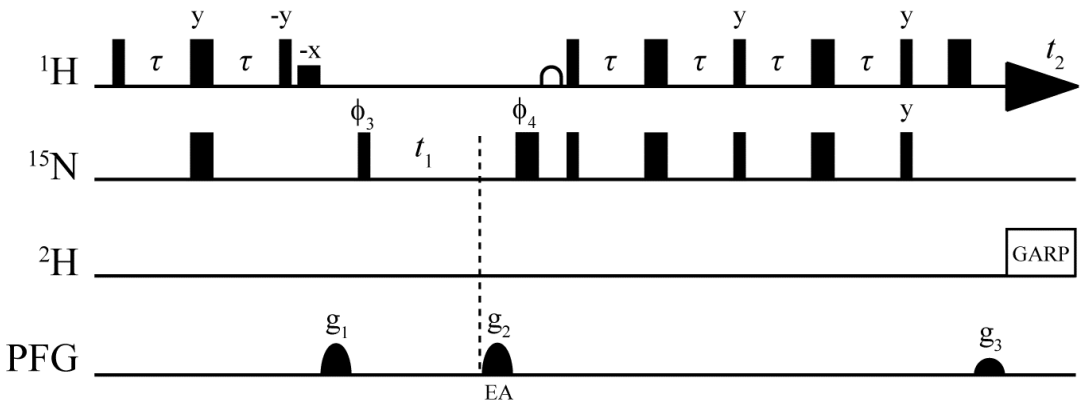

Figure S3: Pulse sequence diagram of the ^{1}H,^{15}N TROSY experiment with variable INEPT delays τ. The sequence is based on the one published by D. Nietlispach [J. Biomol. NMR **31**, 161]. The sequence contains two 90° water flip-back pulses: rectangular pulse with 1 ms duration (small solid rectangle) and E-SNOB pulse with 2.1 ms duration (open rounded rectangle). The phase cycle is ϕ_3=(x,–x), ϕ_4=2(x)2(–x), rec=(x,–x). ^{2}H decoupling during the 80-ms acquisition period is applied with *rf* field strength of 1.1 kHz. The echo-antiecho gradient selection scheme is standard [Kay *et al.* J. Am. Chem. Soc. **114**, 10663]. The gradients are $g1 = (25\ \text{G/cm}, 1\ \text{ms})$, $g2 = (\pm 40\ \text{G/cm}, 1\ \text{ms})$, and $g3 = (4.05\ \text{G/cm}, 1\ \text{ms})$.

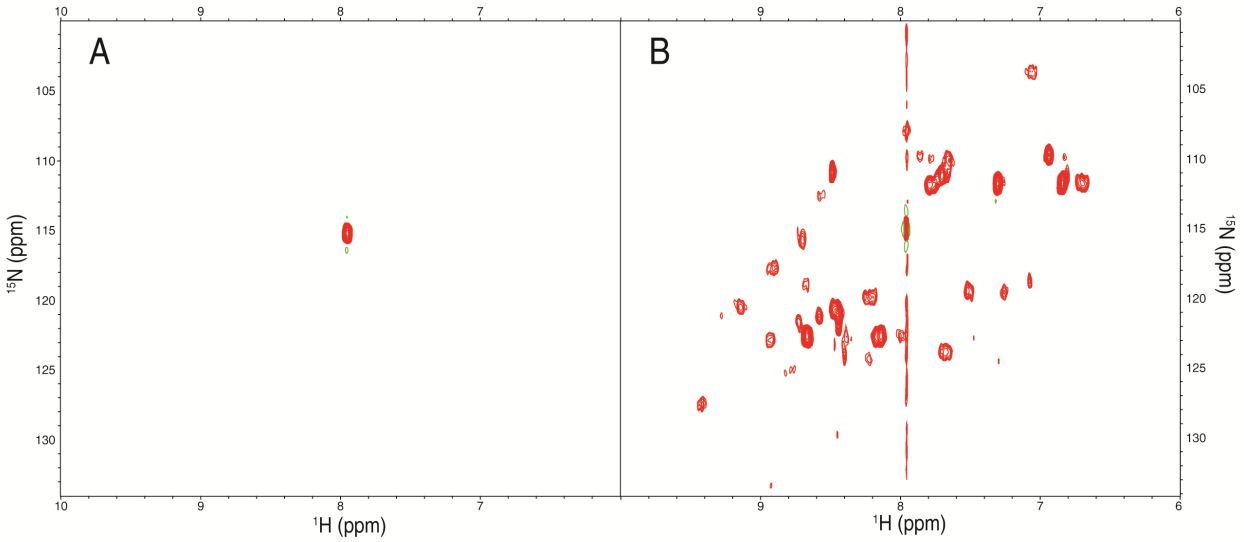

Figure S4: ^{1}H,^{15}N HSQC spectra of (A) 0.4 mM ^{1}H,^{15}N ubiquitin in 12 mg/ml Pf1 phage, 25 mM NaCl, 90% H_2O/10% D_2O and (B) 1.7 mM ^{2}H,^{15}N ubiquitin in 20 mg/ml Pf1 phage, 50 mM NaCl, 25% H_2O/75% D_2O (at 75% content of D_2O, the ubiquitin is observable at an effective concentration of ~0.4 mM [LiWang and Bax *J. Am. Chem. Soc.* **118**, 12864]). Other sample conditions were 10 mM sodium phosphate buffer, pH 7, temperature 298 K. Each spectrum was acquired in 10 minutes at 800 MHz Bruker spectrometer using a standard sensitivity enhanced gradient selected HSQC sequence. The sole peak in panel (A) is from the flexible C-terminal residue G76. In panel (B) this resonance is extremely strong, giving rise to a wiggle-type artifact, which has the appearance of t_1 ridge.

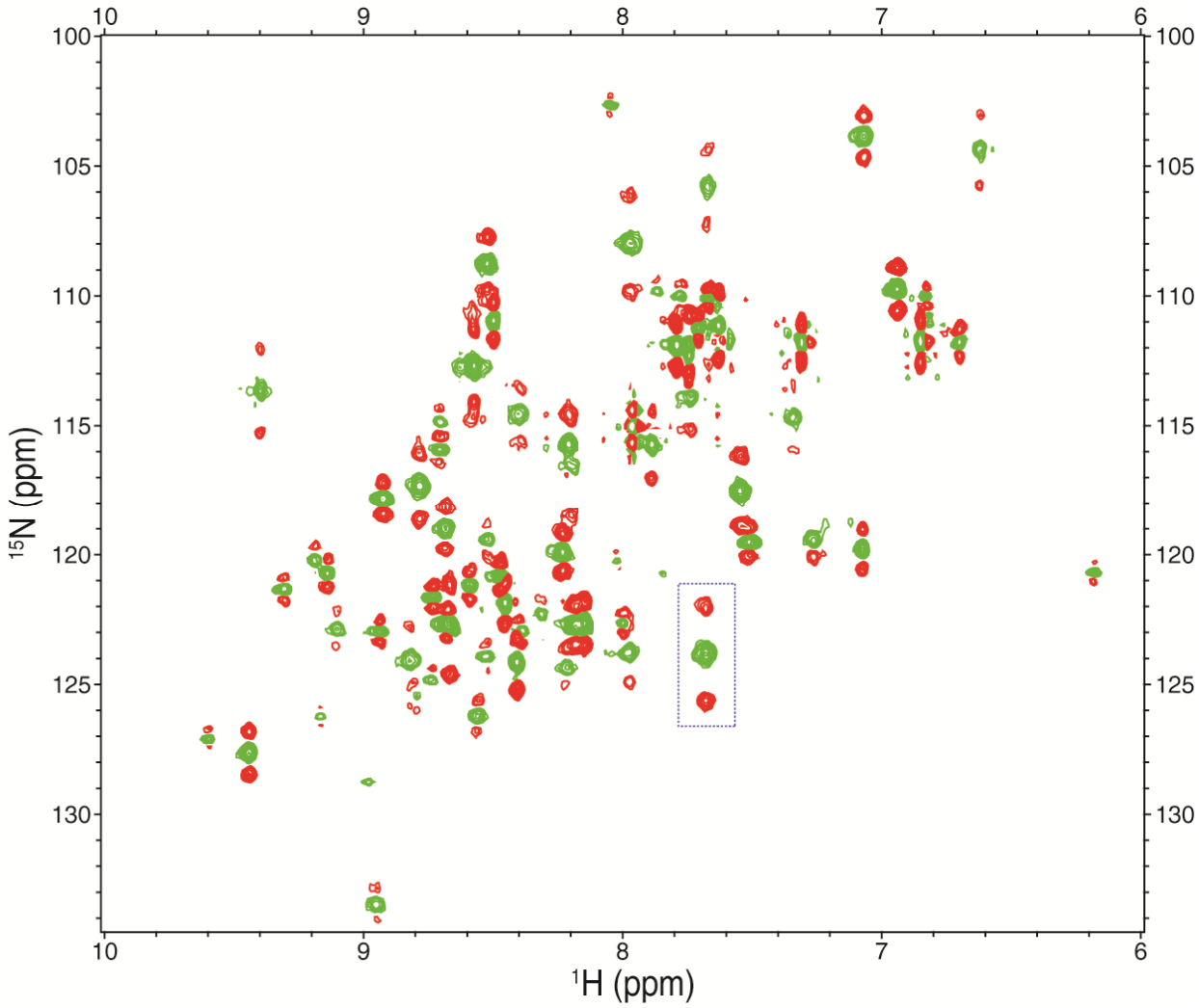

Figure S5: *J*-resolved ^{1}H,^{15}N HSQC spectrum of the strongly aligned ^{2}H,^{15}N ubiquitin. Each resonance represents a triplet, where the central component (negative, green) corresponds to the standard HSQC peak, and the outer components (positive, red) are separated by $|\Sigma| = |{}^{1}J_{NH} + {}^{1}D_{NH}|$. The spectrum was acquired in 5 hrs with 128 complex points in t_1 dimension using the pulse sequence shown in Fig. S1. The peaks enclosed in a dotted-line box are from residue Q62 (this portion of the spectrum is enlarged in Fig. 1 of the text).

	$H\_ + 2H\_N_z$ (broad)	$H\_ - 2H\_N_z$ (sharp)
$N\_ + 2N\_H_z$ (broad)	$\frac{1}{4} I_0 S \chi^2 \left(S^2 \chi + 2S + \chi \right)$	$-\frac{1}{4} I_0 S \chi^3 \left(1 - S^2 \right)$
$N\_ - 2N\_H_z$ (sharp)	$\frac{1}{4} I_0 S \chi^3 \left(1 - S^2 \right)$	$-\frac{1}{4} I_0 S \chi^2 \left(S^2 \chi - 2S + \chi \right)$

Tab. S1. Intensities (volumes) of the four components of $^1H^N$-^{15}N quartet in the TROSY experiment as a function of the variable INEPT duration 2τ. This is an augmented version of Tab. 1, which additionally takes into consideration the attenuation of the signals during the INEPT periods. Given that the protein sample employed in this study is highly deuterated, it can be assumed that the relaxation rates of $^1H^N$ and ^{15}N spins are roughly comparable. Consequently, we assume that all transverse spin modes (e.g. $H\_$, $2H\_N_z$, $N\_$, $2N\_H_z$, $2H\_N\_$, or $2H\_N_+$) decay with one and the same effective rate $R_{2,eff}$, whereas all longitudinal modes do not experience any appreciable relaxation over the time interval on the order of several τ. The short-hand notations used in this table are $S = \sin(\pi \Sigma 2\tau)$ and $\chi = \exp(-R_{2,eff}\, 2\tau)$.

(*next page*)

Figure S6: Peak intensities (volumes) as a function of INEPT delay in *J*-modulated ^1H-^{15}N HSQC series. Initially, 58 backbone resonances have been identified in the spectra. Excluding three resonances that produce poor *autofit* statistics (CHI2>0.1) and two resonances that are heavily overlapped, we arrive at the set of 53 peaks. The $I(\tau)$ data for these peaks together with the best-fit curves obtained by the use of Eq. 2 are shown in the multi-part figure below. Further details can be found in Materials & Methods and in the caption of Fig. 3 (see main text). For those peaks that have not been assigned with a sufficient degree of confidence, the ^1H,^{15}N chemical shifts are indicated in the plot.

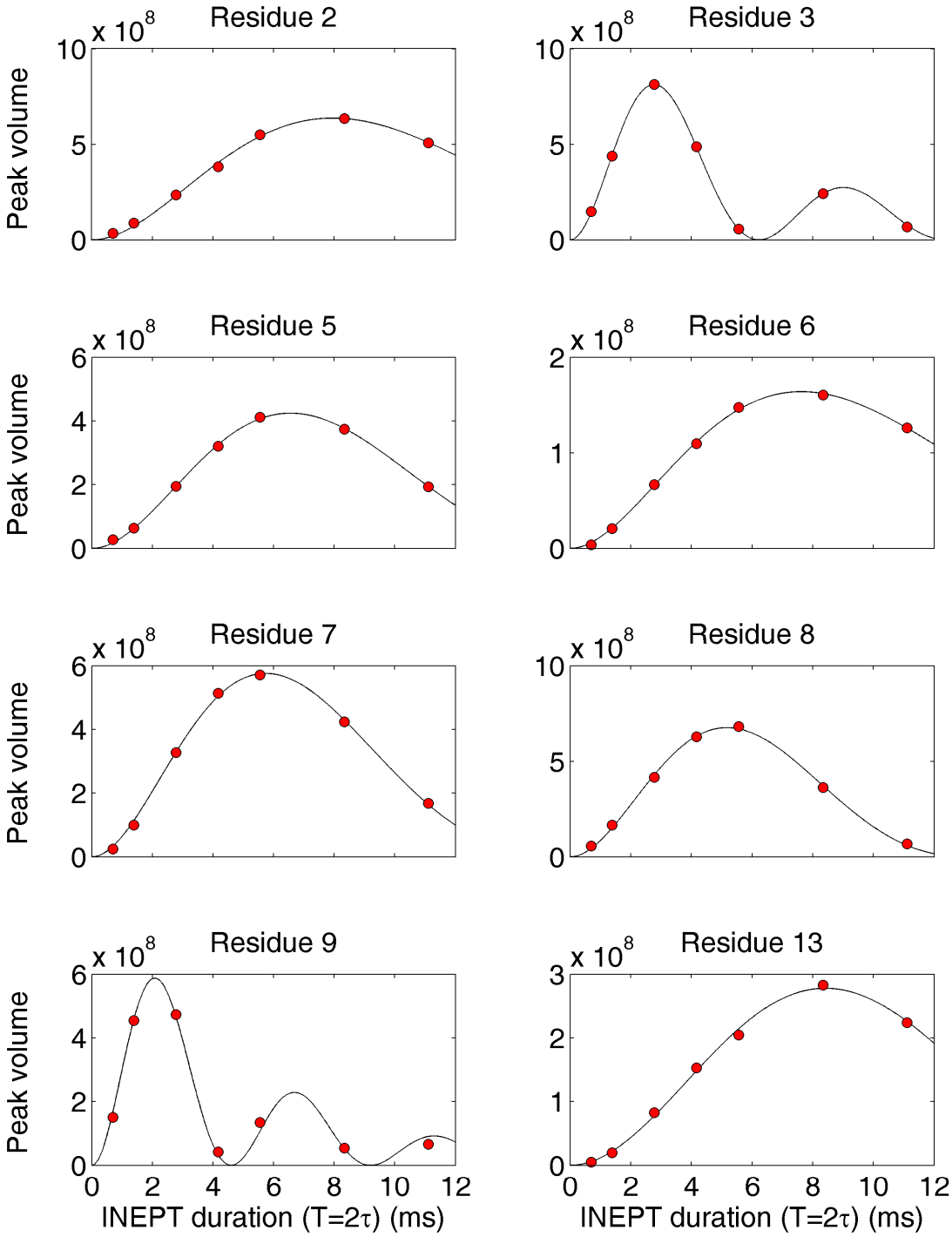

Figure S6: *continued*

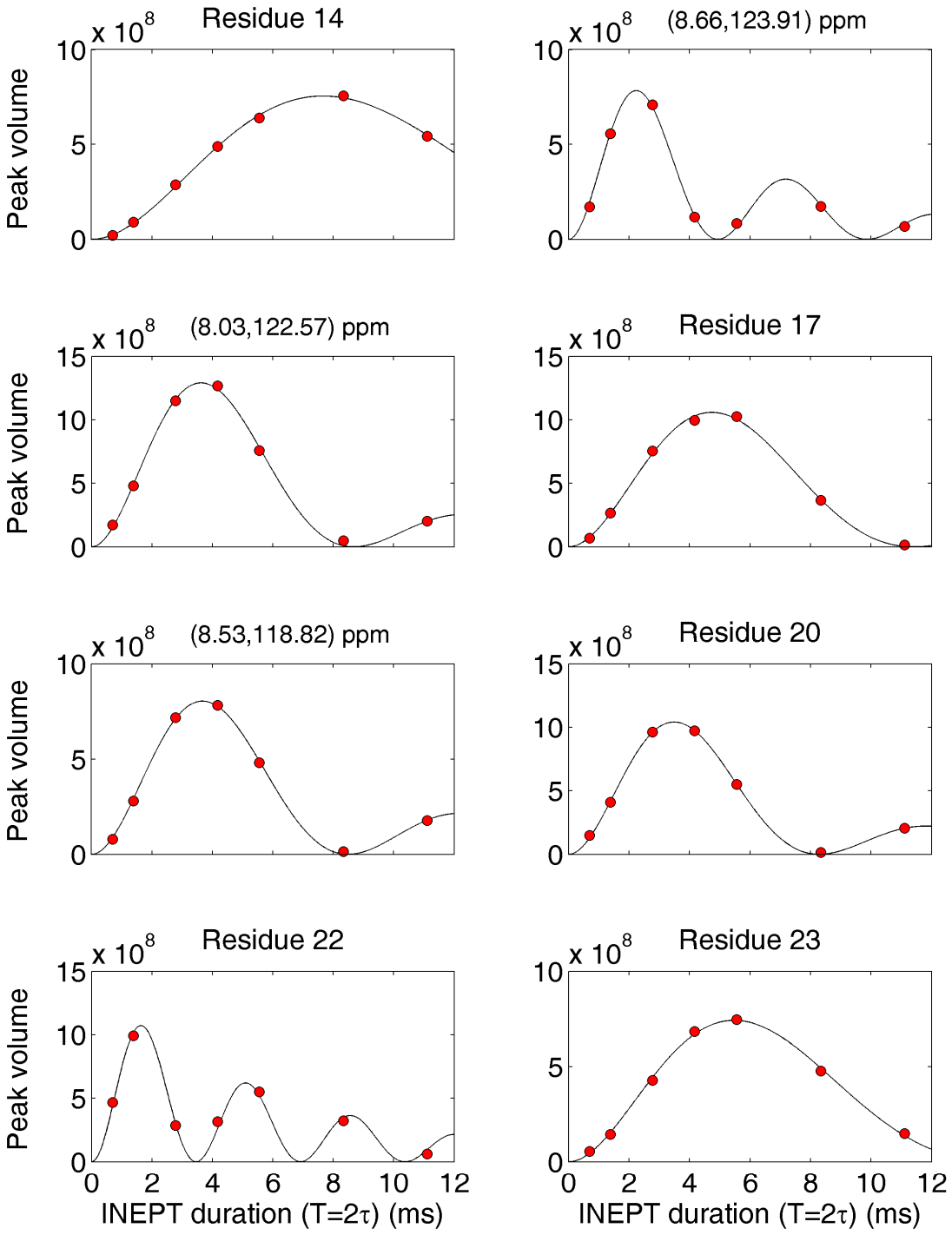

Figure S6: *continued*

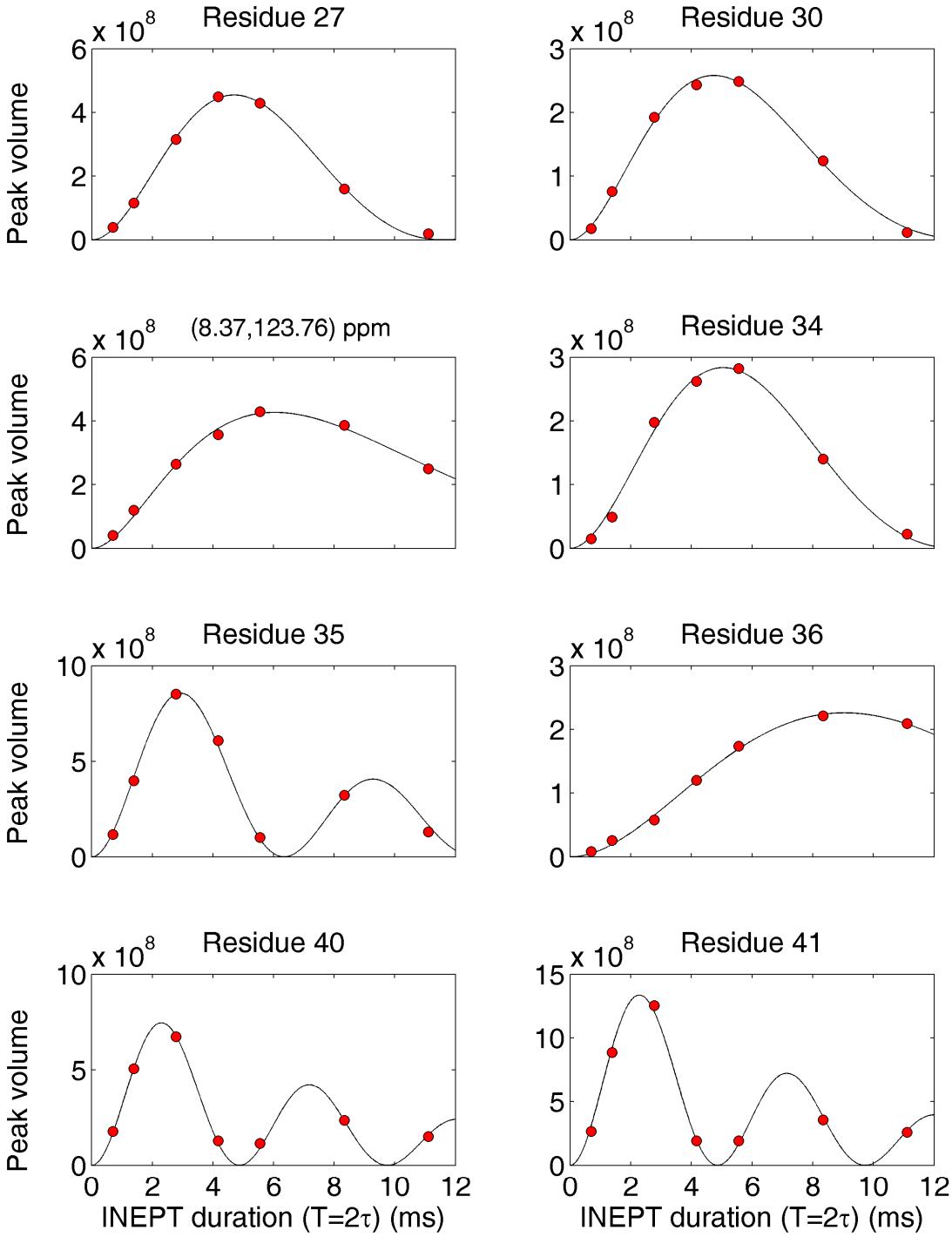

Figure S6: *continued*

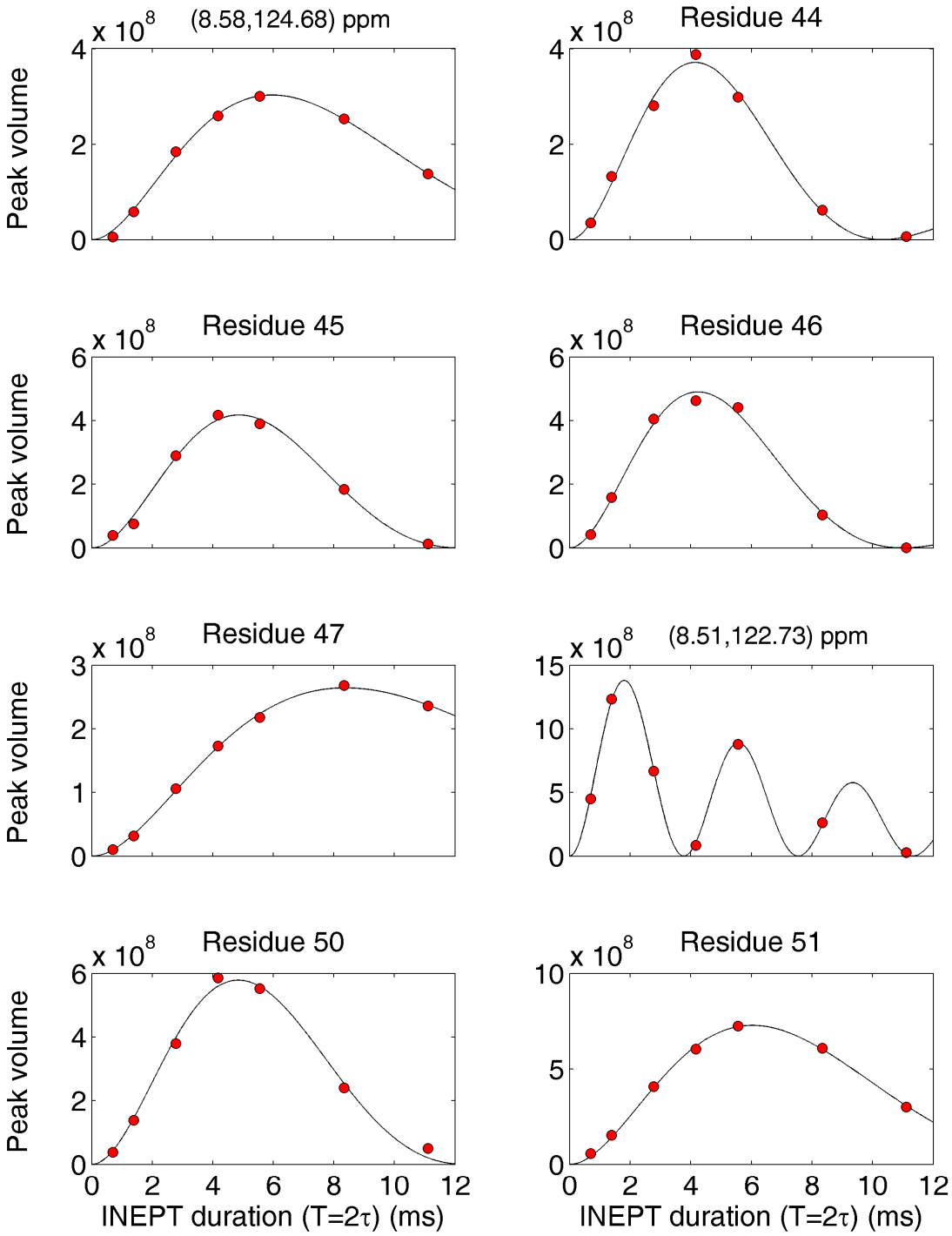
(8.58,124.68) ppm
Residue 44
Residue 45
Residue 46
Residue 47
(8.51,122.73) ppm
Residue 50
Residue 51
x 10^8
Peak volume
INEPT duration (T=2τ) (ms)

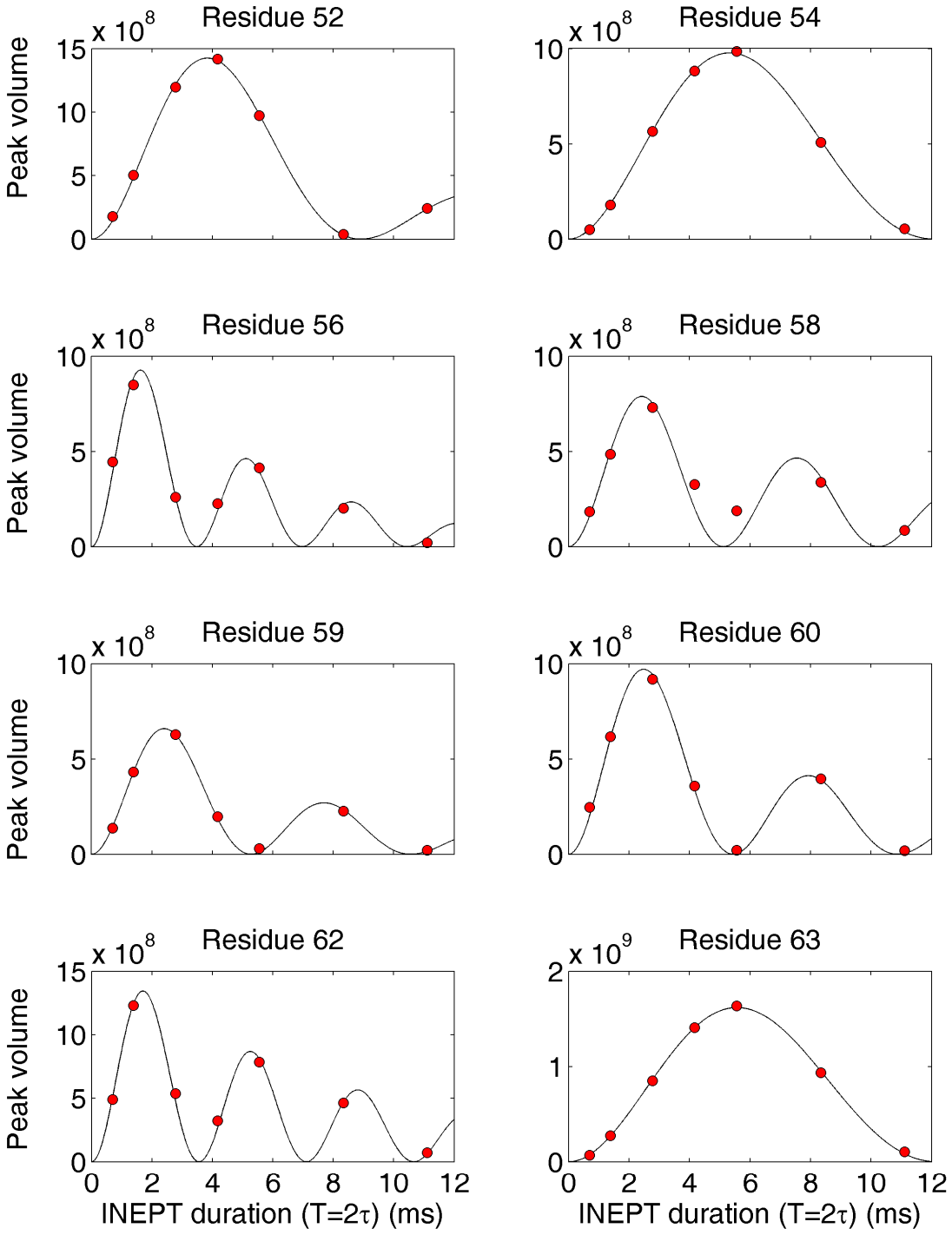

Figure S6: *continued*

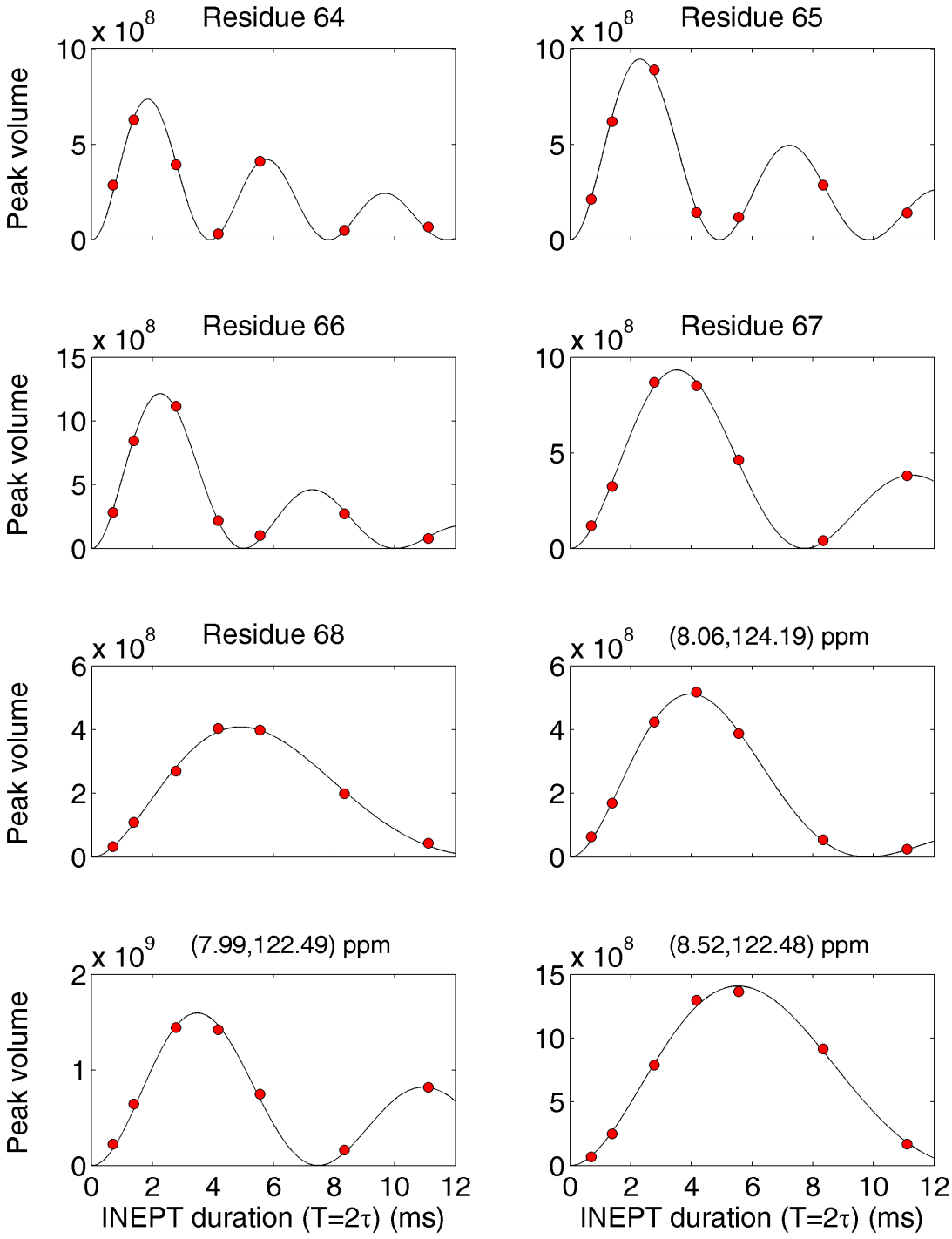

Figure S6: *continued*

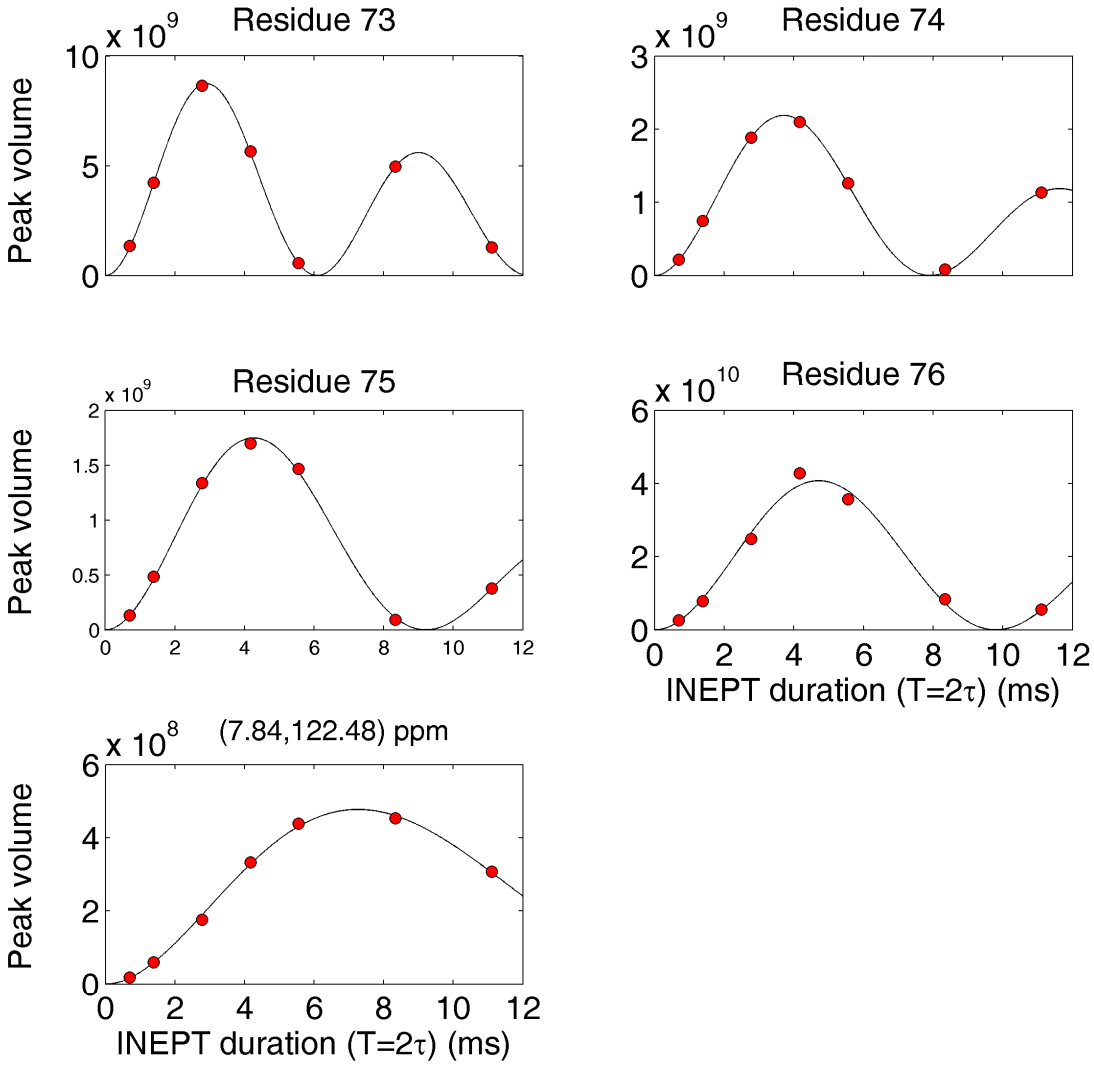

Figure S6: *continued*

Residue number	$^1D_{NH}$ [Hz]	rmsd($^1D_{NH}$) [Hz]
2	44.3	2.0
3	-71.3	2.0
5	31.3	2.4
6	131.5	6.3
7	159.4	0.8
8	18.0	1.8
9	-125.7	1.3
13	48.2	6.5
14	42.1	0.6
17	3.8	1.8
20	-27.5	1.5
22	-193.0	1.8
23	164.9	3.1
27	180.5	0.6
30	165.9	6.0
34	168.4	5.5
35	-64.5	1.3
36	53.7	2.3
40	-108.6	5.7
41	-113.5	1.1
44	189.4	1.5
45	176.1	0.3
46	184.4	2.2
47	126.5	3.0
50	174.1	1.2
51	31.6	4.3
52	-19.4	0.1
54	9.4	0.4
56	-186.2	4.5
58	-92.4	7.1
59	-96.7	3.7
60	-86.6	3.1
62	-186.7	3.5
63	11.5	0.2
64	-158.3	3.1
65	-107.0	4.1
66	-106.4	3.7
67	-36.6	0.4
68	173.3	6.1
70	68.5	3.2

Tab. S2. Assigned $^1D_{NH}$ dipolar couplings from the sample of ubiquitin strongly aligned in Pf1 phage. The couplings represent the average of three values – two derived from ^{1}H and ^{15}N TROSY/HSQC frequency separations and one from HSQC intensity modulation. The last column displays root mean square deviation of these three values (in the case of residue 70, two frequency-based values).

Reference	Sample conditions	Number of $^{1}D_{NH}$ RDCs available for comparison with our data	A_a from fitting with 1UBQ	R from fitting with 1UBQ	α,β,γ from fitting with 1UBQ (deg)
This work	20 mg/ml Pf1 50 mM NaCl pH 7.0 298 K	40	$-1.03\cdot10^{-2}$	0.46	45 / 125 / 215
(Briggman and Tolman 2003)	3.5 mg/ml Pf1 20 mM NaCl pH 6.6 308 K	37	$-2.96\cdot10^{-4}$	0.34	49 / 124 / 220
(Lakomek et al. 2006) *Dataset E5*	15 mg/ml Pf1 400 mM NaCl pH 6.5 308 K	28	$-8.53\cdot10^{-4}$	0.40	56 / 126 / 205
(Lakomek et al. 2006) *Dataset D5*	17 mg/ml Pf1 350 mM NaCl pH 6.5 308 K	11	$-2.39\cdot10^{-3}$	0.31	36 / 128 / 217

Tab. S3. Alignment tensors of ubiquitin in Pf1 media, as obtained from partial ^{1}H-^{15}N RDC datasets (see Tab. 2 in the text). Euler rotations α, β, and γ are defined according to the program PALES (the sense of rotation is opposite to that used in many other programs).